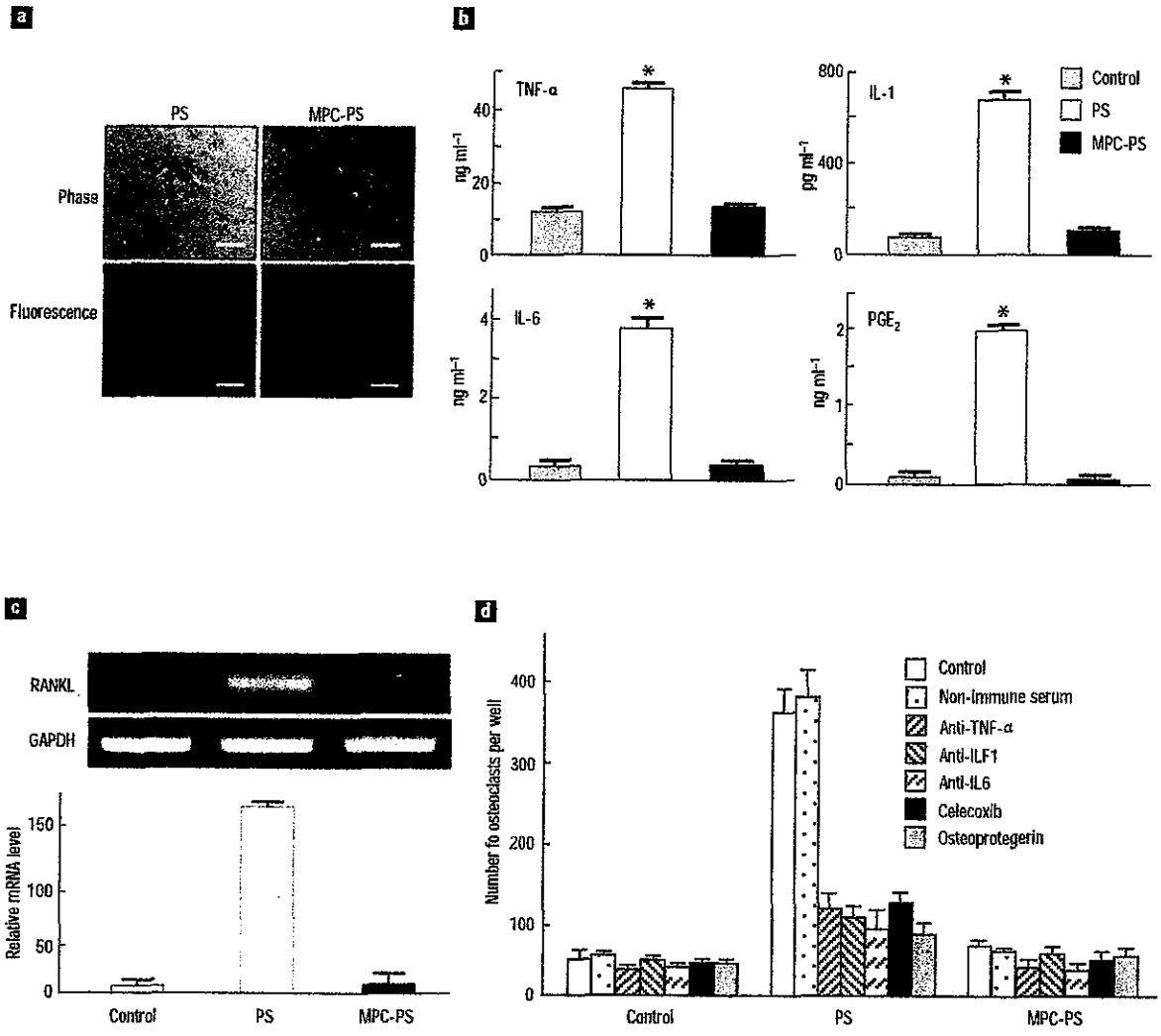

Figure 5 Bone-resorptive responses in cultures exposed to PS particles with and without the MPC grafting (MPC-PS and PS, respectively). **a**, Phagocytosis of fluorescence-labelled particles by cultured mouse intraperitoneal macrophages. Phase: phase contrast microscopic image. Fluorescence: fluorescence microscopic image. Scale bars, 100 μm. **b**, Concentrations of bone-resorptive factors TNF-α, IL-1, IL-6 and PGE_2 in the supernatants of the mouse macrophage-like cell line J774 culture with or without exposure to particles. **c**, RANKL expression by mouse primary osteoblasts isolated from neonatal mouse calvariae and cultured in the three kinds of conditioned media of the J774 cell cultures above. RANKL mRNA levels were determined by semiquantitative RT-PCR (top) and real-time RT-PCR (bottom). GAPDH is glyceraldehyde 3-phosphate dehydrogenase. **d**, Osteoclastogenesis in the coculture of mouse bone marrow cells and osteoblasts by the three kinds of conditioned media of J774 cells above, and inhibition by antagonists to cytokines, PGs and RANKL. Osteoclastogenesis was determined by the number of TRAP-positive multinucleated cells. Data are expressed as means (bars) ± s.e.m. (error bars) for 8–12 cultures per group. * significant difference from control; $P<0.01$.

four- to sixfold by the implantation of non-treated PS particles, as compared with those by the solvent alone, but were little affected by the MPC-grafted particles, indicating that MPC grafting is biologically inert (Fig. 4b).

To further investigate the cellular and molecular mechanisms underlying the prevention of osteoclastic bone resorption by the MPC grafting, we first compared the phagocytosis of fluorescence-labelled PS particles with and without the MPC grafting by cultured mouse intraperitoneal macrophages. Although large amounts of non-treated particles were phagocytosed by macrophages, the MPC-grafted particles were not taken into the cells, probably because biocompatible MPC polymer prevented macrophages from recognizing the particles as foreign bodies (Fig. 5a). We next examined the secretion of bone-resorptive factors by macrophages exposed to the particles. Concentrations of TNF-α, IL-1, IL-6 and PGE_2 in the culture medium of mouse macrophage-like cell line J774 cells were 4–20 times more stimulated by the exposure to non-treated PS particles than those without the exposure; however, the exposure to the MPC-grafted particles affected none of them (Fig. 5b). When the conditioned media of J774 cells were added to a mouse osteoblast culture, the receptor of NF-kB ligand (RANKL) was strongly expressed by the medium exposed to non-treated particles, but not by that exposed to the MPC-grafted particles (Fig. 5c). These results indicate that the MPC grafting prevented the secretion of resorptive factors by macrophages and the subsequent RANKL expression by osteoblasts. Finally, osteoclastogenesis in the coculture of mouse bone marrow cells and osteoblasts was increased about sevenfold by the conditioned medium of J774 cells exposed

to non-treated PS particles as compared with the control, and this stimulation was significantly inhibited by addition of anti-TNF-α, anti-IL-1 or anti-IL-6 antibody, a cyclooxygenase-2 (COX-2) inhibitor celecoxib, and a RANKL inhibitor osteoprotegerin; this confirmed the involvement of some network systems of these factors in the osteoclastogenesis by wear particles. Contrarily, the conditioned medium of J774 cells exposed to the MPC-grafted particles did not increase osteoclastogenesis (Fig. 5d). These biological findings indicate that the MPC grafting can successfully inhibit the bone-resorptive response to wear particles to levels similar to those of recently developed pharmacological therapies such as cytokine antagonists, COX-2 inhibitors and osteoprotegerin[7,8]. Because the lack of side effects of the MPC grafting has already been confirmed clinically by several medical devices[12–14], this surface grafting will surpass the pharmacologic therapies that possibly cause serious side effects during a long period of administration after surgery.

For these biological studies, we initially tried to use the PE wear particles isolated from the hip-simulator experiment above; however, it turned out to be impossible because the PE particles could not be isolated from the lubricants without damaging the MPC polymer layer. The lubricants after loading contain abundant and adhesive proteins that were degraded and precipitated by the heat generated by the head-liner friction. For the isolation of PE particles, it is essential to digest the proteins using strong hydroxide[28,31,32], which cannot avoid breaking the chemical structure such as the esteratic bond of the MPC unit. In fact, the XPS analysis of the surface of isolated particles revealed the lack of the MPC polymer layer. In addition, even if we could isolate the PE particles with MPC grafting properly, the amount from the MPC-CL-PE liner was too small to be used for the biological experiments. We therefore attempted to graft MPC onto the surface of new PE particles or the wear particles from the simulator experiment; however, the floating nature of PE on the liquid surface due to the low specific gravity made the photoinduced polymerization of MPC impossible, because the grafting procedure requires that the particles be agitated in the liquid[29]. Hence, for the biological experiments we used PS particles that have conventionally been used for the *in vivo* and *in vitro* analyses of particle-induced osteolysis as a substitute for PE[6,33,34]. PS is a hydrocarbon polymer just like PE, but has a higher specific gravity than PE. Because these two polymers share similar physical and chemical properties—electrically neutral and little chemical sensitivity—we believe that biological responses to these particles are also similar.

Taken together, the present results demonstrate that grafting MPC onto the PE liner surface of the hip prosthesis markedly decreased the friction and the production of wear particles. In addition, even if the particles were produced by friction, they were biologically inert with respect to phagocytosis by macrophages and subsequent bone-resorptive responses: secretion of cytokines and PGE_2, induction of RANKL, and osteoclastogenesis.

Although this study focused on the hip prosthesis, whose loosening is the most frequent and serious among total joint replacements of upper and lower extremities, the MPC grafting can be used for the prevention of periprosthetic osteolysis of other joints, in which PE particles from articular interfaces are also known to initiate the catabolic cascade[35,36]. From the mechanical and biological advantages shown in this study, we believe that the MPC grafting will make a significant improvement in total joint replacements by preventing periprosthetic osteolysis and aseptic loosening. The development of this technique would improve the quality of care of patients having total joint replacements and have a substantial public health impact. We are now designing a large-scale clinical trial.

METHODS

For mechanical analyses, a 12-station hip-joint wear simulator apparatus (MTS, MTS Systems, Minneapolis, Minnesota) with three kinds of PE liners in 42 mm acetabular cups: non-crosslinked PE liner (K-MAX, Japan Medical Materials, Osaka), crosslinked PE liner (K-MAX Excellink), and MPC-grafted K-MAX Excellink, coupled to 22 mm cobalt–chromium–molybdenum alloy heads (K-MAX HH-02, Excellink), was mounted on rotating blocks to produce biaxial or orbital motion[16]. The simulator experiment was performed according to the international standard of "implants for surgery – wear of total hip-joint prosthesis" established by ISO (#14242-1; 2002), which was proved to be closest to the physiological conditions. Briefly, a Paul-type loading profile, which is a physiological walking simulation with continuous cyclic motion and loading, was applied (maximum force = 280 kgf, frequency = 1 Hz)[37] in the lubricant of distilled water containing 25% bovine calf serum. Friction torque between the liner and the femoral head was measured using a torque measuring instrument. The simulator was run up to 3×10^6 cycles, and the change of lubricant and gravimetric measurement of the liners were performed every 5×10^5 cycles. For the isolation of wear particles, the lubricant after the loading was incubated with 5 N NaOH solution in order to digest adhesive proteins that were degraded and precipitated; the particles were then collected and underwent sequential filtrations, as reported previously[32]. The size of particles was defined as the maximum dimensions by SEM analysis.

For biological analyses, all animal experiments were performed according to the guidelines of the International Association for the Study of Pain[38], and were approved by the committee of Tokyo University charged with confirming ethics. The *in vivo* mouse calvaria experiment was performed as reported previously[7,8]. Briefly, after exposing the calvaria of mice, a subperiosteal injection of PS particles (average diameter = 468 nm; Polysciences, Warrington, Pennsylvania) with or without the MPC grafting, or an equal volume of solvent (deionized water) alone was performed.

Mice were sacrificed seven days after the surgery, and the calvaria was excised, fixed, and decalcified in EDTA. Osteoclastogenesis in the coronal histological sections was determined by TRAP staining. The sections were subjected to histomorphometric analyses under a light microscope with a micrometer, and parameters for bone resorption were measured as reported previously[39]. For the phagocytosis experiment, mouse intraperitoneal macrophages were isolated, exposed to fluorescence-labelled particles, cultured for 1 h, and observed with a fluorescence microscope. Mouse macrophage-like cell line J774 cells (Riken Cell Bank, Saitama, Japan) were exposed to particles and cultured for 24 h. The supernatants were subject to cytokine and PGE_2 measurements using the ELISA method, and were used as the conditioned media for the following assays. For the RANKL expression assay, mouse osteoblasts isolated from neonatal calvariae were cultured in the conditioned media for 24 h. RANKL expression in osteoblasts was measured using the semi-quantitative and real-time reverse transcription polymerase chain reaction (RT-PCR) analyses. The information on the primers is available upon request. For osteoclast formation assay, mouse primary osteoblasts above and bone marrow cells isolated from adult mouse long bones were cocultured in the conditioned media in the presence or absence of anti-TNF-α, anti-IL1, anti-IL-6 antibody, control non-immune serum, celecoxib or osteoprotegerin. Cells were stained with TRAP, and those positively stained and containing more than three nuclei were counted as osteoclasts. For the statistical analysis, means of groups were compared by ANOVA and the significance of differences was determined by post-hoc testing using Bonferroni's method.

Received 13 April 2004; accepted 9 August 2004; published 24 October 2004.

References

1. Harris, W. H. Wear and periprosthetic osteolysis: the problem. *Clin. Orthop.* **393**, 66–70 (2001).
2. Jacobs, J. J., Roebuck, K. A., Archibeck, M., Hallab, N. J. & Glant, T. T. Osteolysis: basic science. *Clin. Orthop.* **393**, 71–77 (2001).
3. Connelly, G. M., Rimnac, C. M., Wright, T. M., Hertzberg, R. W. & Manson, J. A. Fatigue crack propagation behavior of ultrahigh molecular weight polyethylene. *J. Orthop. Res.* **2**, 119–125 (1984).
4. von Knoch, M. *et al.* The effectiveness of polyethylene versus titanium particles in inducing osteolysis in vivo. *J. Orthop. Res.* **22**, 237–243 (2004).
5. Maloney, W. J. *et al.* Isolation and characterization of wear particles generated in patients who have had failure of a hip arthroplasty without cement. *J. Bone Joint Surg. Am.* **77**, 1301–1310 (1995).
6. Glant, T. T. *et al.* Bone resorption activity of particulate-stimulated macrophages. *J. Bone Miner. Res.* **8**, 1071–1079 (1993).
7. Childs, L. M. *et al.* In vivo RANK signaling blockade using the receptor activator of NF-κB:Fc effectively prevents and ameliorates wear debris-induced osteolysis via osteoclast depletion without inhibiting osteogenesis. *J. Bone Miner. Res.* **17**, 192–199 (2002).
8. Goater, J. J., O'Keefe, R. J., Rosier, R. N., Puzas, J. E. & Schwarz, E. M. Efficacy of ex vivo OPG gene therapy in preventing wear debris induced osteolysis. *J. Orthop. Res.* **20**, 169–173 (2002).
9. Ishihara, K., Ueda, T. & Nakabayashi, N. Preparation of phospholipid polymers and their properties as polymer hydrogel membrane. *Polym. J.* **22**, 355–360 (1990).
10. Ishihara, K., Shinozuka, T., Hanazaki, Y., Iwasaki, Y. & Nakabayashi, N. Improvement of blood compatibility on cellulose hemodialysis membrane: IV. Phospholipid polymer bonded to the membrane surface. *J. Biomater. Sci. Polym. Edn* **10**, 271–282 (1999).
11. Yoneyama, T., Sugihara, K., Ishihara, K., Iwasaki, Y. & Nakabayashi, N. The vascular prosthesis without pseudointima prepared by antithrombogenic phospholipid polymer. *Biomaterials* **23**, 1455–1459 (2002).
12. Kihara, S. *et al.* In vivo evaluation of a MPC polymer coated continuous flow left ventricular assist system. *Artif. Organs* **27**, 188–192 (2003).
13. Lewis, A. L. Phosphorylcholine-based polymers and their use in the prevention of biofouling. *Colloids Surf. B* **18**, 261–275 (2000).
14. Lewis, A. L., Tolhurst, L. A. & Stratford, P. W. Analysis of a phosphorylcholine-based polymer coating on a coronary stent pre- and post-implantation. *Biomaterials* **23**, 1697–1706 (2002).
15. Ishihara, K., Iwasaki, Y., Ebihara, S., Shindo, Y. & Nakabayashi, N. Photoinduced graft polymerization of 2-methacryloyloxyethyl phosphorylcholine on polyethylene membrane surface for obtaining blood cell adhesion resistance. *Colloids Surf. B* **18**, 325–335 (2000).
16. Nakamura, T. *et al.* Clinical and laboratory wear studies of zirconia-on-UHMWPE combination in cementless THA. *Key Eng. Mater.* **240–242**, 823–826 (2003).
17. Sochart, D. H. Relationship of acetabular wear to osteolysis and loosening in total hip arthroplasty. *Clin. Orthop.* **363**, 135–150 (1999).
18. Williams, P. F. 3rd, Powell, G. L. & LaBerge, M. Sliding friction analysis of phosphatidylcholine as a boundary lubricant for articular cartilage. *Proc. Inst. Mech. Eng. H* **207**, 59–66 (1993).

19. Hills, B. A. Boundary lubrication in vivo. *Proc. Inst. Mech. Eng. H* **214,** 83–94 (2000).
20. Dowson, D. & Jin, Z. M. Micro-elastohydrodynamic lubrication of synovial joints. *Eng. Med.* **15,** 63–65 (1986).
21. Ishihara, K. *et al.* Why do phospholipid polymers reduce protein adsorption? *J. Biomed. Mater. Res.* **39,** 323–330 (1998).
22. Black, J. Metal on metal bearings. A practical alternative to metal on polyethylene total joints? *Clin. Orthop.* **329,** S244–S255 (1996).
23. Callaway, G. H., Flynn, W., Ranawat, C. S. & Sculco, T. P. Fracture of the femoral head after ceramic-on-polyethylene total hip arthroplasty. *J. Arthroplasty* **10,** 855–859 (1995).
24. Wright, T. M., Rimnac, C. M., Faris, P. M. & Bansal, M. Analysis of surface damage in retrieved carbon fiber-reinforced and plain polyethylene tibial components from posterior stabilized total knee replacements. *J. Bone Joint Surg. Am.* **70,** 1312–1319 (1988).
25. Livingston, B. J., Chmell, M. J., Spector, M. & Poss, R. Complications of total hip arthroplasty associated with the use of an acetabular component with a Hylamer liner. *J. Bone Joint Surg. Am.* **79,** 1529–1538 (1997).
26. Kurtz, S. M., Muratoglu, O. K., Evans, M. & Edidin, A. A. Advances in the processing, sterilization, and crosslinking of ultra-high molecular weight polyethylene for total joint arthroplasty. *Biomaterials* **20,** 1659–1688 (1999).
27. McKellop, H., Shen, F. W., DiMaio, W. & Lancaster, J. G. Wear of gumma-crosslinked polyethylene acetabular cups against roughened femoral balls. *Clin. Orthop.* **369,** 73–82 (1999).
28. Ingram, J. H., Stone, M., Fisher, J. & Ingham, E. The influence of molecular weight, crosslinking and counterface roughness on TNF-alpha production by macrophages in response to ultra high molecular weight polyethylene particles. *Biomaterials* **25,** 3511–3522 (2004).
29. Konno, T., Kurita, K., Iwasaki, Y., Nakabayashi, N. & Ishihara, K. Preparation of nanoparticles composed with bioinspired 2-methacryloyloxyethyl phosphorylcholine polymer. *Biomaterials* **22,** 1883–1889 (2001).
30. Boyce, B. F., Aufdemorte, T. B., Garrett, I. R., Yates, A. J. & Mundy, G. R. Effects of interleukin-1 on bone turnover in normal mice. *Endocrinology* **125,** 1142–1150 (1989).
31. Campbell, P. *et al.* Isolation of predominantly submicron-sized UHMWPE wear particles from periprosthetic tissues. *J. Biomed. Mater. Res.* **29,** 127–131 (1995).
32. Jono, K., Takigawa, Y., Takadama, H., Mizuno, M. & Nakamura, T. A multi-station hip joint simulator study and wear characterization of commercial hip endoprostheses. *Ceram. Eng. Sci. Proc.* **24,** 255–260 (2003).
33. Vernes, C. *et al.* The effects of particulate wear debris, cytokines, and growth factors on the functions of MG-63 osteoblasts. *J. Bone Joint Surg. Am. A* **83,** 201–211 (2001).
34. Yao, J., Cs-Szabo, G., Jacobs, J. J., Kuettner, K. E. & Glant, T. T. Suppression of osteoblast function by titanium particles. *J. Bone Joint Surg. Am.* **79,** 107–112 (1997).
35. Inagaki, K. *et al.* Importance of a radial head component in Sorbie unlinked total elbow arthroplasty. *Clin. Orthop.* **400,** 123–131 (2002).
36. Shanbhag, A. S. *et al.* Quantitative analysis of ultrahigh molecular weight polyethylene (UHMWPE) wear debris associated with total knee replacements. *J. Biomed. Mater. Res.* **53,** 100–110 (2000).
37. Paul, J. P. Forces transmitted by joints in the human body. *Proc. Inst. Mech. Eng.* **181,** 8–15 (1967).
38. Zimmermann, M. Ethical guidelines for investigations of experimental pain in conscious animals. *Pain* **16,** 109–110 (1983).
39. Ogata, N. *et al.* Insulin receptor substrate-1 in osteoblast is indispensable for maintaining bone turnover. *J. Clin. Invest.* **105,** 935–943 (2000).

Acknowledgements

We thank Noboru Yamawaki, Takatoshi Miyashita, Hiroaki Takadama, Kaori Jono, Reiko Yamaguchi, and Mizue Ikeuchi for their excellent technical help. This work was supported by Grants-in-Aid for Scientific Research from the Japanese Ministry of Education, Culture, Sports, Science and Technology (#15390449), and Health and Welfare Research Grant for Comprehensive Research on Aging and Health from the Japanese Ministry of Health, Labour and Welfare.
Correspondence and requests for materials should be addressed to H.K.
Supplementary Information accompanies the paper on www.nature.com/naturematerials

Competing financial interests

The authors declare that they have no competing financial interests.

Regulation of Enzyme−Substrate Complexation by a Substrate Conjugated with a Phospholipid Polymer

Keigo Takei, Tomohiro Konno, Junji Watanabe, and Kazuhiko Ishihara*

Department of Materials Engineering, School of Engineering, The University of Tokyo, 7-3-1, Hongo, Bunkyo-ku, Tokyo 113-8656, Japan

Received October 24, 2003; Revised Manuscript Received January 29, 2004

To recognize and control ligand−receptor interactions at the interface between cells and polymer materials, we investigated a model system with an enzyme and a substrate conjugated with a biocompatible phospholipid polymer in an aqueous medium. We explored the regulation of enzyme−substrate (ES) complexation using horseradish peroxidase (HRP) as the enzyme and 4-aminoantipyrine (AAP) and 3-(*p*-hydroxyphenyl) propionic acid (HPPA) as substrates. The phospholipid polymer (PMBN), composed of 2-methacryloyloxyethyl phosphorylcholine, *n*-butyl methacrylate, and *p*-nitrophenyloxycarbonyl poly(oxyethylene)methacrylate, was prepared and conjugated with AAP (PMBN−AAP conjugate). The formation and dissociation of the ES complex were investigated using capillary electrophoresis and fluorescence spectroscopy. In the chart of the capillary electrophoresis, a much longer retention time of HRP was observed in the PMBN−AAP conjugate-coated capillary compared with that in a nontreated capillary. The retention time was significantly longer in comparison with the case of a mixed solution of HRP and AAP. This result clearly shows that HRP forms an ES complex with the immobilized PMBN−AAP conjugate and that the addition of AAP to the medium inhibits the interactions between HRP and the PMBN−AAP conjugate. Though HRP forms an ES complex with both AAP and the PMBN−AAP conjugate, the ES complex with the PMBN−AAP conjugate was easily dissociated by addition of HPPA as an alternative substrate because HRP started to react with the HPPA immediately. However, the HRP that formed an ES complex with AAP fell behind in reacting with the HPPA. The activity of HRP was maintained at the initial level in the presence of the PMBN−AAP conjugate at 25 °C for 1 week. Additionally, even under H_2O_2 conditions, HRP stored with the PMBN−AAP conjugate maintained 40% of the initial activity whereas HRP was deactivated within 6 h. This result indicates that the PMBN−AAP conjugate could block the active sites by formation of an ES complex. This is due to the formation of the ES complex, which retained the structure of HRP by blocking the active sites. On the basis of these results, we considered that the reversible attachment and detachment by PMBN conjugated with specific ligands from cellular receptors will be realized.

Introduction

Cell adhesion to an extracellular matrix (ECM) is necessary for subsequent cell functions such as proliferation and differentiation.[1] Cells can form tissues, which are mediated by the interactions between ligands on the ECM and receptors on the cell membrane. These interactions impart regulation of the cell functions. However, in vitro, conventional polymer materials such as polystyrene, polyurethane, and poly(ethylene terephthalate), which are produced inexpensively on an industrial scale, have been used for cell and tissue engineering. In general, cell growth was observed on these conventional materials; however, there is a possibility of causing an inflammatory reaction.[2] Additionally, when different kinds of cells are cocultured on these materials, one is surrounded by the other or one of them cannot survive because of the difference in proliferation potencies or adhesive properties.[3,4] Therefore, new suitable materials that can mimic the functions of ECM and impart regularities such as temporal and spatial controls to cells should be designed for tissue regeneration in vitro.

The final goal of this study is regulation of the timing to start cell adhesion on material surfaces. This can be achieved by using a water-soluble polymer conjugated with ligands. Water-soluble ligand molecules such as Arg-Gly-Asp-Ser prevent adhesion of cells on material surfaces,[5] but those cells can never adhere again. On the contrary, ligands conjugated to the polymer backbone could form a complex with cellular receptors and prevent adhesion of cells temporarily, but the addition of free ligand molecules could dissociate the complex and allow the cells to adhere to the material. We explored the possibility of this "reversible blocking of cellular receptors with artificial ligands" using the enzyme−substrate (ES) complexation as a fundamental tool (Figure 1). An enzymatic reaction can be considered a low molecular model of the interaction between cellular receptors and specific ligands. Both are reactions in which a protein reacts with specific molecules; that is, the ES complex corresponds to a receptor−ligand complex.

* To whom correspondence should be addressed. Tel.: +81-3-5841-7124. Fax: +81-3-5841-8647. E-mail: ishihara@bmw.t.u-tokyo.ac.jp.

10.1021/bm0344250 CCC: $27.50
Published on Web 03/10/2004

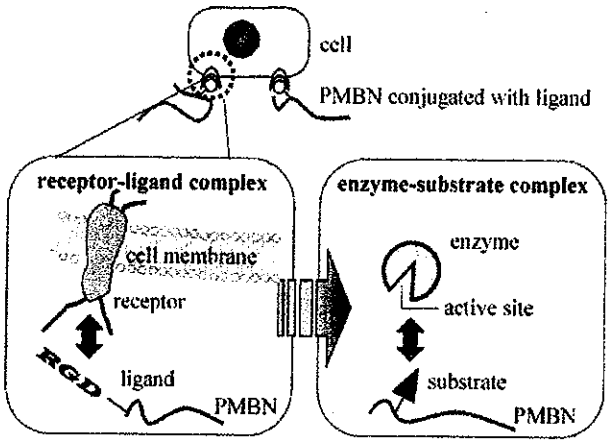

Figure 1. ES complex as a receptor–ligand model.

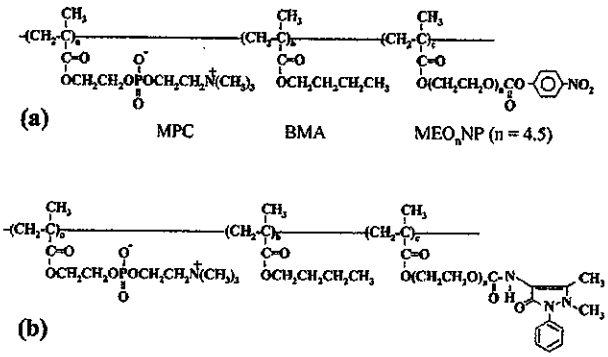

Figure 2. Chemical structures of (a) PMBN and (b) the PMBN–AAP conjugate.

For this purpose, the polymer is required to be bioinert. Polymers composed of 2-methacryloyloxyethyl phosphorylcholine (MPC) and *n*-butyl methacrylate (BMA) suppress not only protein adsorption and cell adhesion but also the inflammatory reaction to adherent cells.[6–8] This is due to the fact that the MPC has the same polar group as the phosphatidylcholines that are typical phospholipids mainly located at the outer surface of the cell membrane.[9] The surface of the MPC polymer shows excellent biocompatibility. In addition to its bioinert nature, the polymer is also required to be able to conjugate with specific molecules. With this in mind, a novel phospholipid polymer (PMBN, Figure 2a) composed of MPC, BMA, and *p*-nitrophenyloxycarbonyl poly(oxyethylene)methacrylate (MEONP) was designed.[10] One of the monomer units, the MEONP unit, has an active ester group in the side chain, so it can conjugate with specific biomolecules via a urethane bond.[11,12]

It has already been reported that an enzyme conjugated with a phospholipid polymer shows the high stability,[13] but the effects of a phospholipid polymer conjugated with substrates on enzymatic reaction or enzymatic activity have not been clarified yet. In this study, we investigated the effect of a substrate conjugated with the PMBN on the formation and dissociation of an ES complex using horseradish peroxidase (HRP) as the enzyme, 4-aminoantipyrine (AAP) and 3-(*p*-hydroxyphenyl) propionic acid (HPPA) as substrates, and regulation of the enzymatic activity by the PMBN–AAP conjugate. This idea will be developed to regulate cell adhesion for cell and tissue engineering.

HRP has a high stability and is widely used in the enzyme-linked immunosorbent assay.[14] The enzymatic reaction of HRP can be observed with a UV detector, because both HPR and the reaction intermediate of HRP have specific absorption spectra.[15] One of the substrates of HRP, HPPA, can be detected with high sensitivity by fluorescence spectroscopy, and AAP has an amine group and can conjugate to PMBN.

Capillary electrophoresis was utilized as an affinity capillary electrophoresis, which can recognize specific molecules and specific affinity interactions such as ES and DNA interactions.[16] In this study, interaction between HRP and AAP was estimated by capillary electrophoresis.

Experimental Section

Materials. Poly(oxyethylene) monomethacrylate (MEOOH) obtained from NOF Co., Ltd., (Tokyo, Japan) was used without further purification. The average number of repeating units in the poly(oxyethylene) chain of MEOOH was 4.5 as determined by ^{1}H NMR (JEOL JNM-GX 270, Tokyo, Japan) spectroscopy. BMA (Wako Pure Chemicals Co., Ltd., Osaka, Japan) was purified by distillation under a reduced pressure, and the fraction of bp 63 °C/24 mmHg was used. MPC was synthesized by a previously described method and used after recrystallization from acetonitrile.[17] *p*-Nitrophenylchloroformate was purchased from Sigma-Aldrich, Co. (St. Louis, MO), and HRP (100 units/mg), AAP, and HPPA were from Wako Pure Chemicals and used as received. The other reagents were commercially available and used without further purification.

Synthesis of MEONP and PMBN. One of the monomer units, MEONP, was synthesized as previously described.[10] Briefly, equimolar amounts of MEOOH and triethylamine (TEA) were added to *p*-nitrophenylchloroformate dissolved in chloroform at −30 °C. The precipitate in the mixture, which was triethylamine hydrochloride, was filtered off, and the solvent was evaporated under a reduced pressure. After addition of dry diethyl ether to the residue, filtration and evaporation were repeated twice and MEONP was then obtained. The chemical structure of MEONP was confirmed by Fourier transform infrared spectoscopy (FT/IR-615, Jasco, Tokyo, Japan) and ^{1}H NMR (JEOL AL300, Tokyo, Japan). Poly(MPC-*co*-BMA-*co*-MEONP) (PMBN*a*: "*a*" represents the MPC unit mol % in the PMBN) was synthesized by a conventional radical polymerization in ethanol solvent using 2,2′-azobisisobutyronitrile as an initiator.[18] By analysis of phosphorus and *p*-nitrophenol, the composition of each monomer unit in PMBN was determined, and the molecular weight of PMBN was evaluated by gel-permeation chromatography (column: OHpak SB-803 HQ, Shodex, Tokyo, Japan) with poly(ethylene oxide) (PEO) standards.

Conjugation with the Substrate. Water-soluble PMBN40 was dissolved in 2 mL of aqueous AAP solution containing 100 mg of AAP. The final concentration of PMBN40 was 50 mg/mL. The solutions were kept under three different conditions: at 37 °C for 48 h, at 37 °C for 24 h, and at room temperature for 24 h. In the case of water-insoluble PMBN30, ethanol was used as a solvent. After conjugation, 0.1 M NaOH solution was added to the solutions to hydrolyze

Table 1. Synthetic Results for PMBN[a]

	monomer unit composition (mol %)							
	in feed			in polymer[b]				
code	MPC	BMA	MEONP	MPC	BMA	MEONP	M_w[c]	solubility in water[d]
PMBN30	30	65	5	27	61	12	3.8×10^4	–
PMBN40	40	50	10	38	47	15	3.6×10^4	+

[a] [Monomer] = 1.0 M, [AIBN] = 10 mM in ethanol, temperature = 60 °C. [b] Determined by analysis of phosphorus and *p*-nitrophenol. [c] Determined by GPC in water/CH_3OH = 3:7, PEO standards. [d] Solubility was determined with 10 mg/mL of each polymer sample and described as soluble (+) and insoluble (–).

the remaining active ester groups. Low-molecular-weight byproducts and unreacted AAP were removed by a dialysis membrane (molecular weight cutoff: 10 000, Pierce, Rockford, IL) with double-distilled deionized water for 2 days. The PMBN–AAP conjugate (Figure 2b) was obtained by lyophilization. The amount of AAP contained in the PMBN–AAP conjugate was determined by fitting to the calibration curve of AAP for absorbance at 265 nm. The Michaelis constant (K_m) was evaluated by the reaction of three PMBN40–AAP conjugates, which have different amounts of AAP, and was compared with that of AAP. The K_m value was determined from the increase in absorbance at 415 nm that was derived from the reaction intermediate.

Formation of the ES Complex. Formation of the ES complex was examined by measuring the retention time of HRP by capillary electrophoresis (CAPI-3300, Otsuka Electronics, Osaka, Japan). An ethanol solution of 0.5 wt % PMBN30–AAP conjugate was allowed to flow through the capillary whose internal diameter was 75 μm and length was 50 cm, and then the ethanol was vaporized by a flowing air flush. These processes were repeated twice, and we obtained the capillary coated with the PMBN30–AAP conjugate. The capillary was maintained at 25 °C and charged at 6 kV. The HRP solution (0.5 mg/mL), 18 mM AAP solution, and the mixed solution of the HRP and AAP (concentration of HRP and AAP were 0.5 mg/mL and 18 mM, respectively) were electrophoresed for 30 min and detected with a UV detector at 200 nm. Phosphate-buffered saline (PBS, 100 mM, pH = 7.1) was used as the medium for electrophoresis.

Dissociation of ES Complex. Dissociation of the ES complex was examined by fluorescence spectroscopy (FP-6500, Jasco, Tokyo, Japan). The ES complex was formed by mixing an equal amount of 0.1 mg/mL HRP solution with various AAP solutions (including the PMBN40–AAP conjugate). Fifty microliters of those solutions was then added to 1.5 mL of the 3.6 μM HPPA solution. The ES complex formed between HRP and AAP was dissociated by the addition of HPPA. On addition of the 0.3 mg/mL H_2O_2 solution (25 μL), the reaction started, and an increase in fluorescence intensity at 404 nm, which indicates the reaction of HPPA, was observed. On the basis of this fluorescence intensity, the enzymatic activity of HRP stored with the PMBN40–AAP conjugate was also measured, and the effect of the ES complex on the enzymatic activities was investigated.

Results and Discussion

Synthesis Results for PMBN. The synthesis results for PMBN are shown in Table 1. The weight average molecular weight (M_w) was roughly 4×10^4 based on PEO standards. The monomer unit composition was quantitatively related to the feeding ratio. The polymer having about 40 unit mol % of MPC, PMBN40, could be dissolved in water, but the polymer with 30 unit mol % of MPC (PMBN30) had insufficient solubility in water. The solubility of the polymer in water depends on the MPC unit composition.

Table 2. Results of Conjugation with AAP under Various Conditions

sample	time (h)	temperature (°C)	AAP concentration[a] (mM)	conversion[b] (%)
PMBN40–AAP(L)	24	22	3.6×10^{-2}	5.7
PMBN40–AAP(M)	24	37	6.59×10^{-2}	11.2
PMBN40–AAP(H)	48	37	13.6×10^{-2}	23.0

[a] AAP concentration when the polymer concentration was 1 mg/mL. [b] 100% means that all active ester groups react with AAP.

AAP Conjugation. The amount of AAP in 1 mg/mL PMBN40–AAP solution varied from 3.4×10^{-2} to 1.4×10^{-1} mM on changing the conditions of conjugation. Table 2 shows that the amount of AAP incorporated in the polymer was dependent on the temperature and reaction time. The obtained conjugates were abbreviated as follows: [PMBN40–AAP(H), PMBN40–AAP(M), and PMBN40–AAP(L), respectively]. When the PMBN40–AAP(H) conjugate was dissolved in water at 1 mg/mL, the concentration of AAP was 1.36×10^{-1} mM. In the PMBN40–AAP(H) conjugate, 23% of the active ester groups was converted to AAP. These concentrations of AAP in the three conjugates were sufficient for the enzymatic reaction, which was estimated using free AAP and HRP. The K_m value of the PMBN–AAP conjugate was 1.1×10^{-5} M, and this value was about one-tenth that of AAP (2.0×10^{-4} M). This result indicates that the affinity of the PMBN40–AAP conjugate for HRP is higher than that of AAP. This is because the local concentration of AAP in the PMBN–AAP conjugate became high as a result of immobilization. The PMBN40–AAP(H) conjugate was used in the following experiments.

Capillary Electrophoresis. In Figure 3, the retention time of HRP, AAP, and the mixed solution of the HRP and AAP in electrophoresis is shown. In the case of the nontreated capillary, the retention time of the HRP was similar to that of AAP. However, using a capillary coated with the PMBN30–AAP conjugate, HRP was detected about 2 min later than AAP, while electrophoresis of HRP with AAP showed no delay in the retention time. In the case of the mixed solution, both charts were almost the same. These results indicate that the elution of HRP is delayed by the interaction with the PMBN30–AAP conjugate immobilized

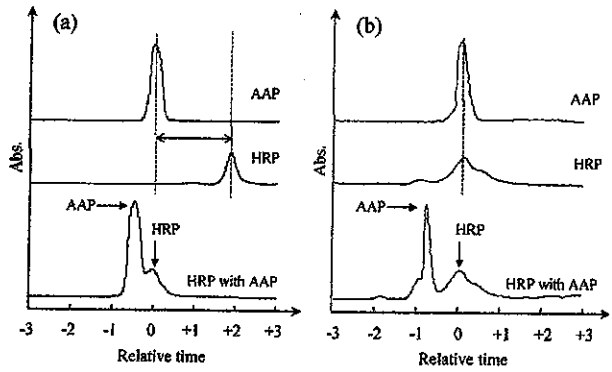

Figure 3. Retention times of HRP, AAP, and the mixed solution of HRP and AAP by electrophoresis (a) using a PMBN30–AAP conjugate-coated capillary and (b) using a nontreated capillary.

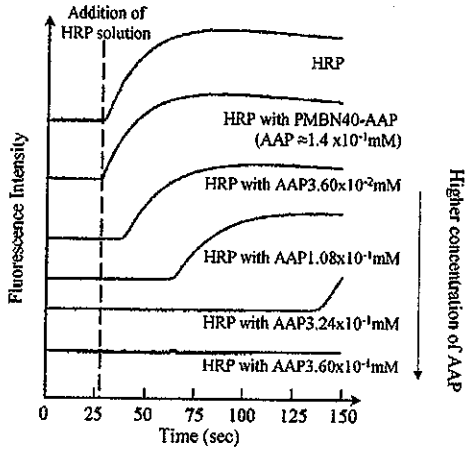

Figure 4. Time prior to starting the enzymatic reaction of HPPA by addition of various HRP solutions.

inside of the capillary, but the addition of the AAP inhibits this interaction by forming the ES complex before electrophoresis. It is considered that the PMBN–AAP conjugate has an ability to form an ES complex with the HRP. With AAP, the PMBN–AAP conjugate could not form the ES complex with the HRP because the ability of AAP to form the ES complex was decreased by conjugation with PMBN. Therefore, the PMBN30–AAP conjugate can block the active sites of HRP temporarily and the ES complex with the PMBN30–AAP conjugate would be easily dissociated by changing the surrounding conditions.

Fluorescence Spectroscopy. Figure 4 shows the change in the fluorescence intensity at 404 nm with the addition of various HRP solutions into HPPA. The increase in fluorescence intensity indicates that the enzymatic reaction occurs between HRP and HPPA. When the mixed solution of HRP and AAP was added to HPPA, the time prior to starting the reaction was delayed, and a time lag appeared that was dependent on the concentration of AAP. The high concentration of AAP prevented the reaction of HPPA with HRP, so HRP reacted with AAP first. The concentration of AAP became low and HPPA was then allowed to react. However, in the case of the PMBN40–AAP conjugate, HPPA immediately reacted, though the amount of AAP equaled the 1.4×10^{-1} mM solution of AAP. This result shows that binding interactions of the ES complex between HRP and the PMBN40–AAP conjugate were not as strong as with

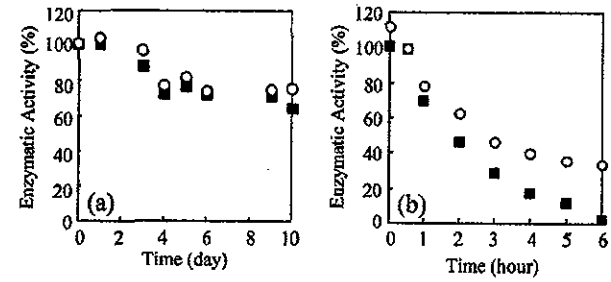

Figure 5. Change in enzymatic activity of HRP incubated with the PMBN40–AAP conjugate in PBS at 25 °C (a) without H_2O_2 and (b) with H_2O_2. The symbols represent (■) native and (○) PMBN40–AAP-(H).

the combination of HRP and AAP. Considering the K_m value, because the affinity of the PMBN40–AAP conjugate for HRP is higher than that of AAP, a decrease in the binding force was caused by the change in mobility of AAP by conjugation to PMBN.

The change in the enzymatic activity of HRP is shown in Figure 5. Under the PBS condition, the activity of HRP was maintained for 1 week, and the existence of the PMBN40–AAP conjugate was not unfavorable for HRP. When stored with H_2O_2, HRP was deactivated within 6 h but the PMBN40–AAP conjugate sustained the HRP activity and 40% of the initial level was maintained. Considering that H_2O_2 affects the heme at the active sites of HRP, this result shows that the PMBN40–AAP conjugate can block the active sites of HRP and has the potential to preserve the structure of HRP.

Conclusions

The bioinert phospholipid polymer that can conjugate with specific molecules was prepared for tissue regeneration in vitro. To investigate the possibility of reversible blocking of the cellular receptor by ligands conjugated with PMBN, the regulation of ES complexation by a substrate conjugated with PMBN was explored as a receptor–ligand model. One of the substrates, AAP, could conjugate with PMBN under moderate conditions. The PMBN–AAP conjugate reacted with HRP effectively as a result of the high local concentration. From the capillary electrophoresis, it was shown that the PMBN–AAP conjugate could form a complex with HRP, but the ability to form a complex was decreased by conjugation. From the fluorescence studies, a complex between the PMBN–AAP conjugate and HRP was easily dissociated by the addition of HPPA as an alternative substrate, while the complex between AAP and HRP could not dissociate. The temporary blocking of the active site of the enzyme was realized by conjugating the substrate with PMBN. This is a promising approach to reversibly blocking cellular receptors. It is considered that ligands conjugated with PMBN can form a complex with the cellular receptor, but this complex would be easily dissociated. Through this reversible blocking of the cellular receptor, a regulation of the timing to start cell adhesion on material surfaces can be realized. This technique can be applied to stacking cells in layers. These studies are currently in progress.

Acknowledgment. A part of this study was financially supported by a Grant-in-Aid for The Development of Innovative Technology (13202) from The Ministry of Education, Culture, Sports, Science and Technology, Japan.

References and Notes

(1) Hynes, R. O. *Cell* **1992**, *69*, 11.
(2) Sawada, S.; Shindo, Y.; Sasaki, S.; Watanabe, A.; Iwasaki, Y.; Kato, S.; Akashi, M.; Ishihara, K.; Nakabayashi, N. *Trans. Soc. Biomater.* **1999**, *25*, 231.
(3) Nicol, A.; Garrod, D. R. *J. Cell Sci.* **1979**, *38*, 249.
(4) Bhatia, S. N.; Balis, U. J.; Yarmush, M. L.; Toner, M. *FASEB J.* **1999**, *13*, 1883.
(5) Behravesh, E.; Zygourakis, K.; Mikos, A. G. *J. Biomed. Mater. Res.* **2003**, *65A*, 260.
(6) Ishihara, K.; Tsuji, T.; Sakai, Y.; Nakabayashi, N. *J. Polym. Sci., Part A: Polym. Chem.* **1994**, *32*, 859.
(7) Ishihara, K.; Nomura, H.; Mihara, T.; Kurita, K.; Iwasaki, Y.; Nakabyashi, N. *J. Biomed. Mater. Res.* **1997**, *39*, 323.
(8) Sawada, S.; Sakaki, S.; Iwasaki, Y.; Nakabayashi, N.; Ishihara, K. *J. Biomed. Mater. Res.* **2003**, *64A*, 411.
(9) Ishihara, K.; Nakabayashi, N. *J. Polym. Sci., Part A: Polym. Chem.* **1991**, *29*, 831.
(10) Konno, T.; Watanabe, J.; Ishihara, K. *Biomacromolecules*, in press.
(11) Solovskij, M. V.; Panarin, E. F.; Gorbunova, O. P.; Korneeva, E. V.; Petuhkova, N. A.; Michajlova, N. A.; Pavlov, G. M. *Eur. Polym. J.* **2000**, *36*, 1127.
(12) Torchilin, V. P.; Levchenko, T. S.; Lukyanov, A. N.; Khaw, B. A.; Kilbanov, A. L.; Rammohan, R.; Samokhin, G. P.; Whiteman, K. R. *Biochem. Biophys. Acta* **2001**, *1511*, 397.
(13) Miyamoto, D.; Watanabe, J.; Ishihara, K. *Biomaterials* **2004**, *25*, 71.
(14) Sakaki, S.; Nakabayashi, N.; Ishihara, K. *J. Biomed. Mater. Res.* **1999**, *47*, 523.
(15) Kitagawa, T. In *Spectroscopy of Biological Systems*; Clark, R. J. H., Hester, R. E., Eds.; John Wiley & Sons: New York: 1986; pp 443–481.
(16) Anada, T.; Arisawa, T.; Ozaki, Y.; Takarada, T.; Katayama, Y.; Maeda, M. *Electrophoresis* **2002**, *23*, 2267.
(17) Ishihara, K.; Ueda, T.; Nakabayashi, N. *Polym. J.* **1990**, *22*, 355.
(18) Ueda, T.; Oshida, H.; Kurita, K.; Ishihara, K.; Nakabayashi, N. *Polym. J.* **1992**, *24*, 1259.

BM0344250

PPARγ insufficiency enhances osteogenesis through osteoblast formation from bone marrow progenitors

Toru Akune,[1] Shinsuke Ohba,[2] Satoru Kamekura,[1] Masayuki Yamaguchi,[1] Ung-il Chung,[2] Naoto Kubota,[3] Yasuo Terauchi,[3] Yoshifumi Harada,[4] Yoshiaki Azuma,[4] Kozo Nakamura,[1] Takashi Kadowaki,[3] and Hiroshi Kawaguchi[1]

[1]Department of Orthopaedic Surgery, [2]Department of Tissue Engineering, and [3]Department of Metabolic Diseases, Faculty of Medicine, University of Tokyo, Tokyo, Japan. [4]Teijin Co., Tokyo, Japan.

Based on the fact that aging is associated with a reciprocal decrease of osteogenesis and an increase of adipogenesis in bone marrow and that osteoblasts and adipocytes share a common progenitor, this study investigated the role of PPARγ, a key regulator of adipocyte differentiation, in bone metabolism. Homozygous *PPARγ*-deficient ES cells failed to differentiate into adipocytes, but spontaneously differentiated into osteoblasts, and these were restored by reintroduction of the *PPARγ* gene. Heterozygous *PPARγ*-deficient mice exhibited high bone mass with increased osteoblastogenesis, but normal osteoblast and osteoclast functions, and this effect was not mediated by insulin or leptin. The osteogenic effect of PPARγ haploinsufficiency became prominent with aging but was not changed upon ovariectomy. The PPARγ haploinsufficiency was confirmed to enhance osteoblastogenesis in the bone marrow cell culture but did not affect the cultures of differentiated osteoblasts or osteoclast-lineage cells. This study demonstrates a PPARγ-dependent regulation of bone metabolism in vivo, in that PPARγ insufficiency increases bone mass by stimulating osteoblastogenesis from bone marrow progenitors.

Introduction

Osteoblasts and adipocytes share a common progenitor: multipotential mesenchymal stem cells in bone marrow (1–3). Accumulated evidence of the differentiation switching of these two cell lineages suggests that a large degree of plasticity exists between them and that the relationship is reciprocal (4–6). The clinical fact that a decrease in bone volume (BV) of age-related osteoporosis is accompanied by an increase in marrow adipose tissue (7–9) also implies the possible reciprocal relationship that is postulated to exist between the two differentiation pathways. The signal transduction pathways implicated in this process are therefore evaluated as potential targets for therapeutic intervention of osteoporosis. The molecular mechanism underlying the reciprocal relationship is not yet well understood, however, although several studies using strain-specific and KO murine models have begun to explore the relationship in vivo (10–15).

Several key transcription factors that function in the complex transcriptional cascade during adipocyte differentiation have been identified, including PPARγ and CCAAT enhancer-binding proteins (C/EBPs) (16). PPARγ is a ligand-activated transcription factor that belongs to the nuclear hormone receptor superfamily and functions as a heterodimer with a retinoid X receptor by binding to the PPAR responsive element (PPRE) within the promoters of the target genes (17–19). PPARγ is expressed early in the adipocyte differentiation program and is activated by long-chain fatty acids, peroxisome proliferators, and the thiazolidinedione class of antidiabetic agents (17–19). Most importantly, PPARγ plays requisite and sufficient roles in the regulation of adipocyte differentiation, because its overexpression in fibroblast cell lines initiates adipogenesis (20) and ES cells and embryonic fibroblastic cells from mice lacking *PPARγ* were unable to differentiate into adipocytes (21–23).

When one takes the results of the studies together, it is possible that PPARγ may contribute not only to adipogenesis, but also to osteogenesis in the bone marrow where bipotential precursors can differentiate to either adipocytes or osteoblasts. This study investigated the physiological role of PPARγ on the marrow cells and bone cells using in vivo morphological analyses and ex vivo cell culture systems. For the in vivo analysis, we used mice lacking the *PPARγ* gene, which we generated by gene targeting (22). Although the homozygous *PPARγ*-deficient (*PPARγ*$^{-/-}$) mice were embryonically lethal at 10.5–11.5 days after post coitum due to placental dysfunction, heterozygous *PPARγ*-deficient (*PPARγ*$^{+/-}$) mice developed normally. The heterozygotes led to a 50% reduction in PPARγ expression and exhibited resistance to high-fat diet–induced obesity and insulin resistance; however, on a standard diet they grew normally, without abnormalities in major organs such as brain, heart, liver, spleen, or kidney (22, 24). We show here that the homozygous *PPARγ*-deficient ES cells spontaneously differentiate into osteoblasts ex vivo and that PPARγ haploinsufficiency due to the heterozygous *PPARγ* deficiency resulted in enhanced bone formation with increased osteoblastogenesis from bone marrow progenitors both in vivo and ex vivo.

Methods

Animals. The generation of *PPARγ* gene–targeted mice was described previously (22). In each experiment, WT and *PPARγ*$^{+/-}$

Nonstandard abbreviations used: alkaline phosphatase (ALP); bone morphogenetic protein-2 (BMP-2); bone volume (BV); CCAAT enhancer-binding proteins (C/EBPs); computed tomography (CT); LDL receptor–related protein 5 (LRP5); leukemia inhibitory factor (LIF); M-CSF–dependent bone marrow macrophage (M-BMMϕ); receptor activator of nuclear factor κB ligand (RANKL); ovariectomy (OVX); PPAR responsive element (PPRE); tartrate-resistant acid phosphatase (TRAP); tissue volume (TV); type I collagen α1 chain (COL1A1).

Conflict of interest: The authors have declared that no conflict of interest exists.

Citation for this article: *J. Clin. Invest.* 113:846–855 (2004). doi:10.1172/JCI200419900.

mice littermates fed a standard diet were compared. All experiments were performed on male mice at 8 or 52 weeks of age, except for the ovariectomy (OVX) experiment in which female mice underwent surgical operation at 26 weeks and were analyzed at 30 weeks. All experiments were performed according to the protocol approved by the Animal Care and Use Committee of the University of Tokyo.

ES cell cultures. Mouse *PPARγ*$^{-/-}$ and WT ES cells were isolated from blastocysts generated by mating *PPARγ*$^{+/-}$ mice with each other, as previously described (25). ES cells were maintained in DMEM medium supplemented with 15% FBS, 200 mM L-glutamine, 100 μM β-mercaptoethanol, and 10^3 U/ml of leukemia inhibitory factor (LIF; Chemicon International, Temecula, California, USA). Differentiation of ES cells was induced by using a modified protocol, described previously (2, 26). In brief, after being trypsinized with 0.025% trypsin-EDTA, cells were plated onto a bacterial Petri dish in the absence of LIF and cultured with 100 nM all-*trans* retinoic acid for 5 days, with medium being replenished on day 3. The embryoid bodies were transferred to a gelatinized six-multiwell plate and allowed to adhere to the well with DMEM containing 10% FBS. For the analysis of osteogenic differentiation, cultures were maintained in the same condition without any additional supplements for 10 days, were fixed with 10% buffered formalin, and were incubated in the presence of 5% silver nitrate solution under an ultraviolet light for 10 minutes, then incubated for 5 minutes in the presence of 5% sodium thiosulfate solution (von Kossa staining). To discern the calcified nodules from the embryoid body, both of which are seen as black, the von Kossa–positive nodules that do not connect to the embryoid body in a well were counted. For the analysis of adipogenesis, the medium was supplemented with 1 μM troglitazone (Sankyo Pharmaceutical Co., Tokyo, Japan) for 10 days, fixed in 10 mM sodium periodate, 2% paraformaldehyde, 75 mM L-lysin dihydrochloride, and 37.5 mM sodium phosphate, and then stained in a filtered solution of 0.3% oil red O in 60% isopropanol for 15 minutes. The red-stained, lipid vacuole–containing cells in a well were counted. To rescue osteoblast and adipocyte differentiation of *PPARγ*$^{-/-}$ ES cells, the recombinant retrovirus vector carrying the *PPARγ* gene and empty vector were constructed as previously described (22). ES cells were infected with equal titers of each recombinant virus as described (20), with some modification.

Skeletal morphology and blood chemistry. A bone radiograph was taken with a soft x-ray apparatus (SOFTEX; CMB-2, Tokyo, Japan). A three-dimensional CT scan was taken using a composite x-ray analyzing system (NX-HCP; NS-ELEX Inc., Tokyo, Japan) and the trabecular bone area (percentage of BV per tissue volume [TV]) was measured on the computed tomography (CT) image. All histological analyses were carried out using WT and *PPARγ*$^{-/-}$ littermates as previously described (27). Parameters for the trabecular bone and the number of bone marrow adipocytes was measured in an area 1.2 mm in length from 0.5 mm below the growth plate at the proximal metaphysis of the tibiae. The number of adipocytes in this area was determined by counting that of oval vacuoles in the toluidine blue staining. The thickness of the growth plate was measured at the proximal tibiae. Serum insulin was measured by insulin immunoassay (Morinaga Institute of Biological Science, Yokohama, Japan), and leptin was assayed with the ELISA-based Quantikine M mouse leptin immunoassay kit (R&D Systems Inc., Minneapolis, Minnesota, USA).

Primary bone marrow cell cultures. Bone marrow cells were collected from long bones of 8-week-old *PPARγ*$^{-/-}$ and WT male littermates. Cells were plated at a density of 10^6 cells on a six-multiwell plate in α-MEM containing 10% FBS, with 1 μM troglitazone for the adipogenesis assay and with 50 μg/ml ascorbic acid and 10 mM β-glycerophosphate for osteogenesis assay. The oil red O staining was performed as mentioned above at 14 days of culture. For the alkaline phosphatase (ALP), cultured plates were rinsed with PBS, fixed in 100% ethanol at 10 days of culture, and stained with Tris-HCl–buffered solution (pH 9.0) containing naphthol AS-MX phosphate as a substrate and Fast Blue BB salt (Sigma-Aldrich, St. Louis, Missouri, USA) as a coupler. For the Alizarin red S staining, cultured plates were rinsed with PBS at 21 days of culture, fixed in 10% buffered formalin, and stained with 2% Alizarin red S (pH 4.0) (Sigma-Aldrich). The von Kossa staining was performed as mentioned above at 28 days of culture. For the growth curve assay, bone marrow cells derived from either WT or *PPARγ*$^{-/-}$ littermates were inoculated at a density of 10^7 cells per dish in 10-cm culture dishes in α-MEM containing 10% FBS, 50 μg/ml ascorbic acid, and 10 mM β-glycerophosphate, and then was cultured for 3 days. The adherent cells were then harvested and inoculated at a density of 3×10^5 cells/dish in 10-cm culture dishes and further cultured in the same medium. The number of cells per dish was counted 1, 2, 3, and 4 days after the seeding.

Real-time quantitative RT-PCR. Total RNA was extracted with an ISOGEN kit (Wako Pure Chemicals Industry Ltd., Osaka, Japan), according to the manufacturer's instructions, from ES cells cultured for 10 days after the embryoid bodies were transferred to gelatinized plates and from bone marrow cells cultured for 14 days after the seeding. One microgram of RNA was reverse-transcribed using a Takara RNA PCR Kit (AMV) ver. 2.1 (Takara Shuzo Co., Shiga, Japan) to make single-stranded cDNA. PCR was performed on an ABI Prism 7000 Sequence Detection System (Applied Biosystems Inc., Foster City, California, USA). The PCR reactions consisted of QuantiTect SYBR Green PCR Master Mix (QIAGEN, Tokyo, Japan), 0.3 μM specific primers, and 500 ng of cDNA. Relative levels of mRNA of a specific gene were calculated using the standard curve generated with cDNA dilutions, with normalization to actin as an internal control. PCR primers of specific genes used for amplification are available upon request.

Primary osteoblastic cell cultures. Osteoblastic cells were isolated from calvariae of neonatal WT and *PPARγ*$^{-/-}$ littermates as previously described (27). For the cell proliferation assay, cells were inoculated at a density of 10^4 cells/well in a 24-multiwell plate, cultured in the same medium for 48 hours, and deprived of serum for 12 hours before adding the experimental medium with and without troglitazone (1 μM) or FGF-2 (1 nM; Kaken Pharmaceutical Co., Chiba, Japan). Incorporation of [^{3}H]-thymidine (1 μCi/ml in the medium) added for the final 3 hours was measured after 24 hours of culture. For ALP activity measurement, cells were inoculated at a density of 10^4 cells/well in a 24-multiwell plate and cultured in α-MEM containing 10% FBS and 50 μg/ml ascorbic acid with and without troglitazone (1 μM) or bone morphogenetic protein-2 (BMP-2; 30 ng/ml; Yamanouchi Pharmaceutical Co., Tokyo, Japan). At 14 days of culture, cells were sonicated in 10 mM Tris-HCl buffer (pH 8.0) containing 1 mM $MgCl_2$ and 0.5% Triton X-100. ALP activity in the lysate was measured using a Wako ALP kit (Wako Pure Chemicals Industry Ltd.), and the protein content was determined using a BCA protein assay reagent (Pierce Chemical Co., Rockford, Illinois, USA). For Alizarin red S and von Kossa stainings, cells were inoculated at a density of 5×10^4 cells/well in a six-multiwell plate in α-MEM containing 10% FBS, 50 μg/ml ascorbic acid, and 10 mM β-glyc-

erophosphate, and were stained at day 21 and 28, respectively, as mentioned above. Difference in maturity between the bone marrow cells and the calvarial osteoblasts was examined by the calcified nodule formation determined by Alizarin red S staining and the osteocalcin expression determined by real-time PCR analysis.

Assays for osteoclastic cells. Tartrate-resistant acid phosphatase-positive (TRAP-positive) multinucleated osteoclasts were generated by coculturing osteoblastic cells (10^4 cells/well) and bone marrow cells (5×10^5 cells/well) derived from either WT or *PPARγ*$^{+/-}$ littermates, as mentioned above, in a 24-multiwell plate in α-MEM containing 10% FBS for 6 days with and without $1,25(OH)_2D_3$ (10 nM), prostaglandin E_2 (100 nM), and IL-11 (10 ng/ml). Cells positively stained for TRAP containing more than three nuclei were counted as osteoclasts. To determine bone resorption activity, osteoclasts formed by the coculture on 0.24% collagen gel coated on 100-mm dishes were digested with 0.2% collagenase solution, and a 1:50 aliquot including osteoclasts was seeded on a dentine slice. After 48 hours of culture in α-MEM containing 10% FBS, the total area of pits stained with 0.5% toluidine blue was evaluated using an image analyzer. To study the role of PPARγ intrinsic to osteoclastic cells, we used the M-CSF–dependent bone marrow macrophage (M-BMMϕ) culture system as described previously (28). Briefly, bone marrow cells from WT or *PPARγ*$^{+/-}$ mice were seeded at a density of 3×10^5 cells/well in a 24-multiwell plate and cultured in α-MEM containing 10% FBS with M-CSF (100 ng/ml). After culturing for 3 days, adherent cells (M-BMMϕ) were further cultured with M-CSF (100 ng/ml) and soluble receptor activator of nuclear factor κB ligand (RANKL) (100 ng/ml) for 3 days. TRAP-positive osteoclasts were counted. To determine the survival, osteoclasts generated as above were deprived of M-CSF/soluble RANKL and cultured for an additional 48 hours. At 3, 6, 12, 24, and 48 hours, the TRAP-positive and trypan blue–negative osteoclasts were counted.

Statistical analysis. Means of groups were compared by ANOVA, and significance of differences was determined by post-hoc testing using Bonferroni's method.

Results

Osteogenesis is enhanced in the homozygous PPARγ-deficient ES cell culture. To examine the involvement of the PPARγ signaling in fat and bone metabolism, we first compared the adipogenesis and osteogenesis in

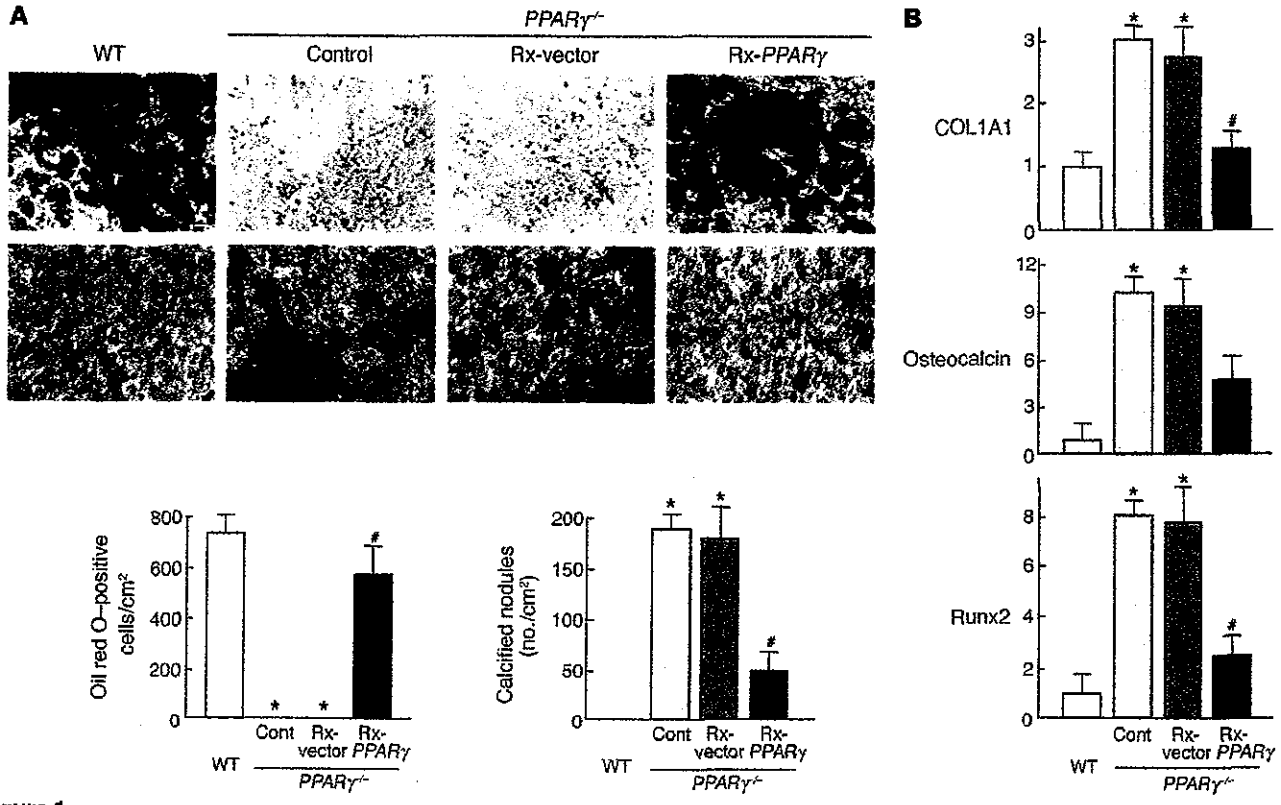

Figure 1

Adipogenesis and osteogenesis in the mouse ES cell cultures of homozygous *PPARγ*-deficient (*PPARγ*$^{-/-}$) and WT genotypes. As a rescue experiment, PPARγ was reintroduced into *PPARγ*$^{-/-}$ ES cells using a retrovirus vector carrying the *PPARγ* gene (Rx-*PPARγ*) or the same retrovirus vector without the *PPARγ* gene (Rx-vector) as a control. (**A**) The upper row shows the adipogenesis determined by the oil red O staining of the ES cell culture in DMEM/10% FBS with troglitazone. The number of oil red O–positive cells stained in red was counted and shown in the left graph as the cells per square centimeter. The images in the lower row indicate the osteogenesis determined by the von Kossa staining of the ES cell culture in DMEM/10% FBS without any osteogenic supplements. The number of von Kossa–positive calcified nodules stained in black was counted and shown in the right graph as the number per square centimeter. Scale bar: 20 μm. (**B**) Relative mRNA levels of the marker genes for osteoblasts — COL1A1, osteocalcin and Runx2 — determined by real-time quantitative RT-PCR 10 days after the embryoid bodies were transferred to a gelatinized six-multiwell plate in DMEM/10% FBS without any osteogenic supplements. The ordinate axis indicates the relative amount of mRNA as compared with that of WT. Data are expressed as means (bars) ± SEMs (error bars) for eight wells per group. *Significant difference from the WT culture, $P < 0.01$. #Significant restoration by Rx-*PPARγ* as compared with the control *PPARγ*$^{-/-}$ and *PPARγ*$^{-/-}$ plus Rx-vector cultures; $P < 0.01$. Cont, control.

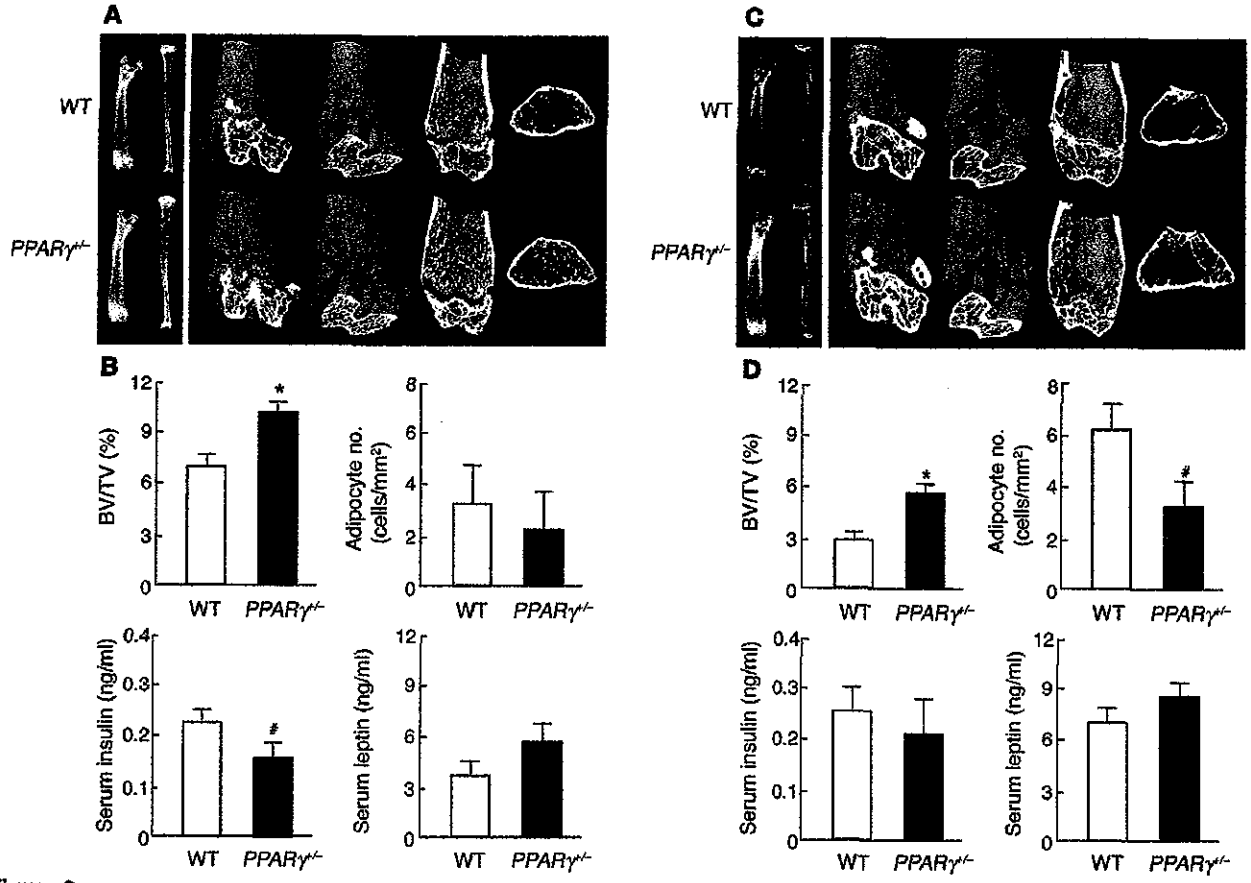

Figure 2

Radiological analysis and blood chemistry of heterozygous *PPARγ*-deficient (*PPARγ*$^{+/-}$) and WT littermates at 8 weeks (**A** and **B**) and 52 weeks (**C** and **D**) of age. (**A** and **C**) Plain x-ray images of femora and tibiae (left) and three-dimensional CT images of distal femora (right) of representative *PPARγ*$^{+/-}$ and WT littermates. (**B** and **D**) Trabecular BV expressed as percentage of total tissue volume (BV/TV [%]) at the distal femora was measured on the CT image. The number of adipocytes in the bone marrow, measured histologically, is shown here for collation with the BV/TV data. Insulin and leptin levels in serum taken just before the sacrifice were quantified using immunoassay kits. Data are expressed as means (bars) ± SEMs (error bars) for eight mice per group for *PPARγ*$^{+/-}$ and WT mice. Significant difference from WT: $^{*}P < 0.01$, $^{\#}P < 0.05$.

the cultures of ES cells between *PPARγ*$^{-/-}$ and WT (WT or *PPARγ*$^{+/+}$) genotypes isolated from blastocysts generated by mating *PPARγ*$^{+/-}$ mice (Figure 1A). In the presence of troglitazone, a thiazolidinedione that is a potent ligand of PPARγ, a substantial amount of oil red O–positive adipocytes was formed from WT ES cells, whereas adipogenesis was not seen in the *PPARγ*$^{-/-}$ ES cell culture (Figure 1A, upper row of photographs). To confirm the direct association between PPARγ and adipogenesis, PPARγ was reintroduced into *PPARγ*$^{-/-}$ ES cells using a retrovirus vector carrying the *PPARγ* gene (Rx-*PPARγ*). Adipogenesis was restored to the level similar to that of WT culture, although introduction of the same retrovirus vector without the *PPARγ* gene (Rx-vector) did not affect it. We then examined the osteogenesis in the *PPARγ*$^{-/-}$ and WT ES cell cultures. Surprisingly, in DMEM/10% FBS without osteogenic supplements such as dexamethasone, β-glycerophosphate, ascorbic acid, or BMP, the formation of von Kossa–positive bone nodules was potently induced in the *PPARγ*$^{-/-}$ ES cell culture, while this was not seen at all in the WT culture (Figure 1A, lower row of photographs). Quantitative analysis of the mRNA levels by the real-time RT-PCR method revealed that the marker genes for osteoblasts — type I collagen α1 chain (COL1A1), osteocalcin, and Runx2 — were upregulated in the *PPARγ*$^{-/-}$ ES cell culture as compared with the WT culture (Figure 1B). Reintroduction of PPARγ into the *PPARγ*$^{-/-}$ culture by Rx-*PPARγ* significantly decreased the nodule formation and osteogenic marker gene expressions, while the control Rx-vector altered neither (Figure 1, A and B). When one takes these results together, the observed mirror image regulations between adipogenesis and osteogenesis by loss and gain of the PPARγ function suggest a switching mechanism between the two differentiation pathways from common progenitors through the PPARγ signaling.

PPARγ haploinsufficiency leads to high bone mass in vivo. To learn the effect of the PPARγ insufficiency in vivo, we analyzed the bones of *PPARγ*$^{-/-}$ mice because the homozygous deficient fetuses died too early for their skeletal analyses to be performed. *PPARγ*$^{+/-}$ mice showed normal weight gain without visible general lipodystrophy on a standard diet during the observation period of up to 52 weeks of age. The lengths of the trunk and long bones were also similar to those of WT littermates, indicating that PPARγ is not involved in the regulation of skeletal growth. X-ray and three-dimensional CT analyses of femora and tibiae, however, revealed that *PPARγ*$^{+/-}$ mice showed about 40% higher trabecular bone mass than WT littermates at 8 weeks of age (Figure 2, A and B).

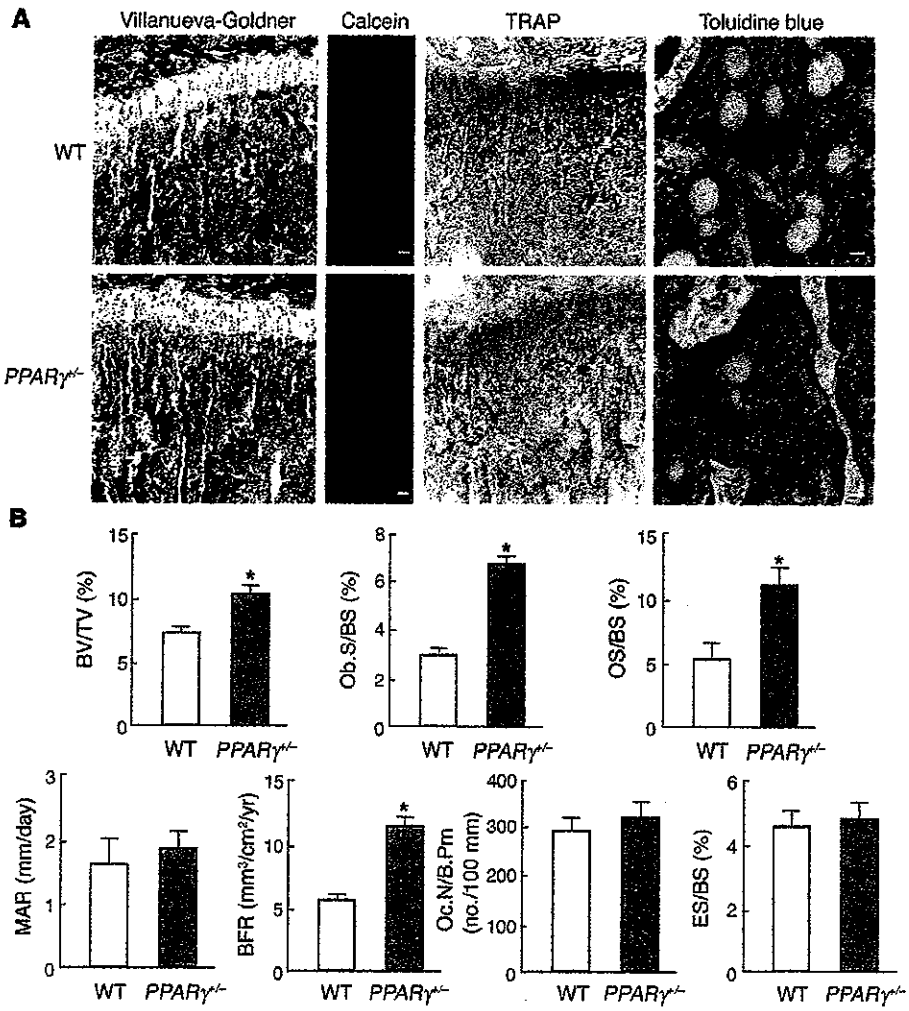

Figure 3
Histological analysis of the proximal tibiae of *PPARγ*$^{+/-}$ and WT littermates. (**A**) Histological features at proximal tibiae of *PPARγ*$^{+/-}$ and WT littermates. Villanueva-Goldner staining, calcein double labeling, and TRAP staining were done at 8 weeks; toluidine blue staining was done at 52 weeks of age. In Villanueva-Goldner staining, mineralized bone is stained green and unmineralized bone osteoid red; scale bar: 100 μm. In calcein double labeling, the mineralization front is stained as a green line; scale bar: 10 μm. In TRAP staining, TRAP-positive osteoclasts are stained red; scale bar: 100 μm. In toluidine blue staining, adipocytes are observed as oval vacuoles; scale bar: 50 μm. (**B**) Histomorphometric parameters at 8 weeks of age. Ob.S/BS, percentage of bone surface covered by cuboidal osteoblasts; OS/BS, percentage of bone surface covered by osteoid; MAR, mineral apposition rate; BFR, bone formation rate expressed by MAR times percentage of bone surface exhibiting double labels plus one-half single labels; Oc.N/B.Pm, number of mature osteoclasts in 100 mm of bone perimeter; ES/BS, percentage of eroded surface. Data are expressed as means (bars) ± SEMs (error bars) for eight mice per group for *PPARγ*$^{+/-}$ and WT mice. *Significant difference from WT, $P < 0.01$.

Contrarily, the number of adipocytes in the bone marrow determined as described below tended to be lower in the *PPARγ*$^{+/-}$ long bones compared with WT (Figure 2B). Similar changes of bone and fat were also seen in vertebral bodies (data not shown). To examine the involvement of systemic factors that are known to be related to bone and fat metabolism, the serum levels of insulin and leptin were compared between the two mouse genotypes. *PPARγ*$^{+/-}$ mice showed lower, although not significantly lower, serum insulin level and higher leptin level than WT littermates as reported previously (22, 29). Since insulin is known to be osteogenic (30), whereas leptin is antiosteogenic (11, 13, 31), neither of the changes in these hormones could explain the increased bone mass in *PPARγ*$^{+/-}$ mice.

Because age-related osteoporosis is known to be accompanied by reciprocal increase of bone marrow adipocytes (7–9), we further compared the bones of *PPARγ*$^{+/-}$ and WT littermates at 52 weeks of age (Figure 2, C and D). The BV of femora and tibiae was decreased in both mouse genotypes at this age as compared with that at 8 weeks; however, the difference of BV between *PPARγ*$^{+/-}$ and WT became more prominent at 52 weeks than at 8 weeks (95% versus 40%, respectively). The number of bone marrow adipocytes, which are shown as oval vacuoles by the toluidine blue staining (Figure 3A, right), was significantly decreased in *PPARγ*$^{+/-}$ mice at this age. This tendency was similarly observed in vertebral bodies (data not shown). Both insulin and leptin levels at this old age showed patterns similar to those at 8 weeks, although significant differences between the genotypes were not seen.

PPARγ haploinsufficiency leads to osteoblastogenesis in vivo. We further performed histological analyses of the proximal tibiae of 8-week-old *PPARγ*$^{+/-}$ mice. Villanueva-Goldner staining indicated increases of trabecular bones stained in green and osteoid surface stained in red in *PPARγ*$^{+/-}$ mice as compared with WT littermates; however, bone formation by individual osteoblasts determined by the calcein double labeling and the number of TRAP-positive osteoclasts was similar for the two groups (Figure 3A). Bone histomorphometric analyses (Figure 3B) confirmed the increase of BV by PPARγ haploinsufficiency to be about 40%. Among bone formation parameters, osteoblast surface and osteoid surface, both representative of the number of osteoblasts, were more than double in *PPARγ*$^{+/-}$ than in WT littermates, while the mineral apposition rate that reflects the bone formation ability of individual osteoblasts did not differ between them. Consequently, bone formation rate that is determined by the number and the function of osteoblasts became about twice that by PPARγ haploinsufficiency. Bone resorption parameters, osteoclast number, and eroded surface did not differ between *PPARγ*$^{+/-}$ and WT mice. Taking these histologi-

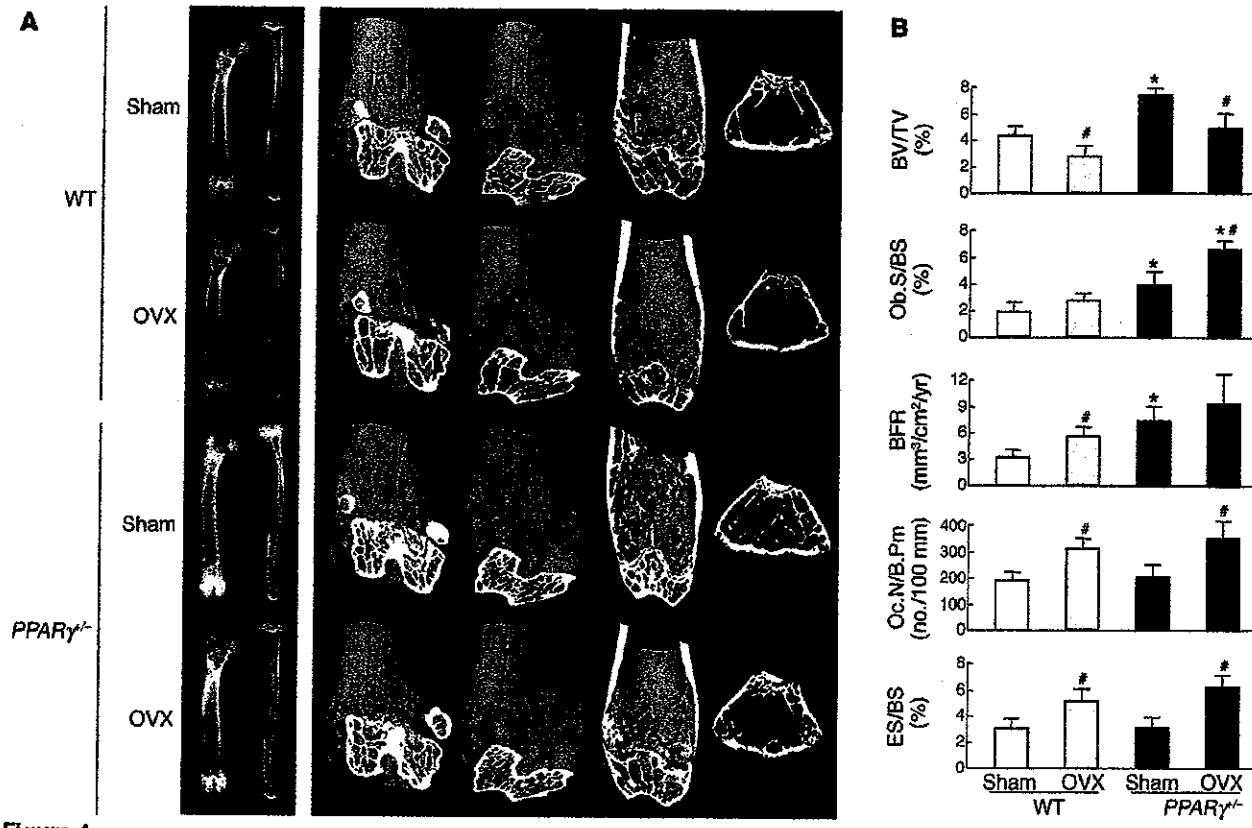

Figure 4
Radiological and histomorphometric analyses of OVX and sham-operated (Sham) female littermates of *PPARγ*$^{+/-}$ and WT genotypes. Female mice underwent surgical operation at 26 weeks and were analyzed at 30 weeks of age. (**A**) Plain x-ray images of femora and tibiae (left) and three-dimensional CT images of distal femora (right) of representative mice. (**B**) Histomorphometric parameters. Data are expressed as means (bars) ± SEMs (error bars) for eight mice per group for *PPARγ*$^{+/-}$ and WT mice. *Significant difference from WT, $P < 0.01$. #Significant difference from sham, $P < 0.05$.

cal observations together, *PPARγ*$^{+/-}$ mice exhibited high bone mass with increased osteoblastogenesis but normal osteoblast and osteoclast functions. The thickness of the growth plate at the proximal tibiae was not different between *PPARγ*$^{+/-}$ and WT littermates (80.4 ± 9.6 and 82.7 ± 10.3 μm, mean ± SEM of eight mice each, respectively), confirming that PPARγ signaling is not important for bone growth through chondrocyte functions.

PPARγ haploinsufficiency does not affect bone loss by OVX. To investigate the involvement of the PPARγ signaling in the mechanism of bone loss by estrogen deficiency, OVX or sham operation was undertaken on 26-week-old female *PPARγ*$^{+/-}$ and WT littermates, and BV was compared 4 weeks after the operation. X-ray and three-dimensional CT analyses of femora and tibiae suggested that both *PPARγ*$^{+/-}$ and WT mice showed similar bone loss by OVX (Figure 4A). Histomorphometric analyses (Figure 4B) showed that BV was about 30% decreased by OVX in both *PPARγ*$^{+/-}$ and WT mice. These decreases were accompanied by increases in bone formation and bone resorption parameters, indicating a state of high bone turnover, in both genotypes. Hence, PPARγ haploinsufficiency did not affect the change of bone metabolism induced by OVX, suggesting that the PPARγ signaling does not contribute to osteopenia caused by estrogen deficiency.

PPARγ haploinsufficiency leads to osteoblastogenesis from cultured bone marrow cells. To investigate the cellular mechanism underlying the abnormality in the bone of *PPARγ*$^{+/-}$ mice, ex vivo cultures of bone marrow cells derived from long bones were performed. We first compared the cell proliferation determined by the growth curve for 4 days and found no difference between *PPARγ*$^{+/-}$ and WT marrow cells (Figure 5A). Adipogenesis from marrow cells in the presence of troglitazone was confirmed to be inhibited by PPARγ haploinsufficiency, however, since the number of oil red O–positive adipocytes was decreased in the *PPARγ*$^{+/-}$ culture to about half that of the WT culture (Figure 5B). We further examined osteoblastogenesis in the bone marrow cell culture by comparing the numbers of colonies positively stained with ALP, Alizarin red S, and von Kossa (Figure 5C). All colonies were markedly increased in the *PPARγ*$^{+/-}$ culture as compared with the WT culture, indicating the increase of osteoblastogenesis from bone marrow progenitors by PPARγ haploinsufficiency.

To further investigate the regulation of expression of genes related to bone metabolism by PPARγ haploinsufficiency, we compared mRNA levels of key or marker molecules for adipocyte and osteoblast differentiations between *PPARγ*$^{+/-}$ and WT bone marrow cells (Figure 5D). As expected, PPARγ expression was reduced in the *PPARγ*$^{+/-}$ marrow cells compared with the WT. The levels of expression of other key factors for adipocyte differentiation, C/EBP-β and C/EBP-δ, in the *PPARγ*$^{+/-}$ marrow cells were comparable to those of WT, indicating that PPARγ was not essential for induction of these C/EBPs; contrarily, C/EBP-α was significantly reduced. Based on previous observations (16, 17, 22, 32, 33) and these results, it appears that C/EBP-β and C/EBP-δ lie upstream of PPARγ, while C/EBP-α is

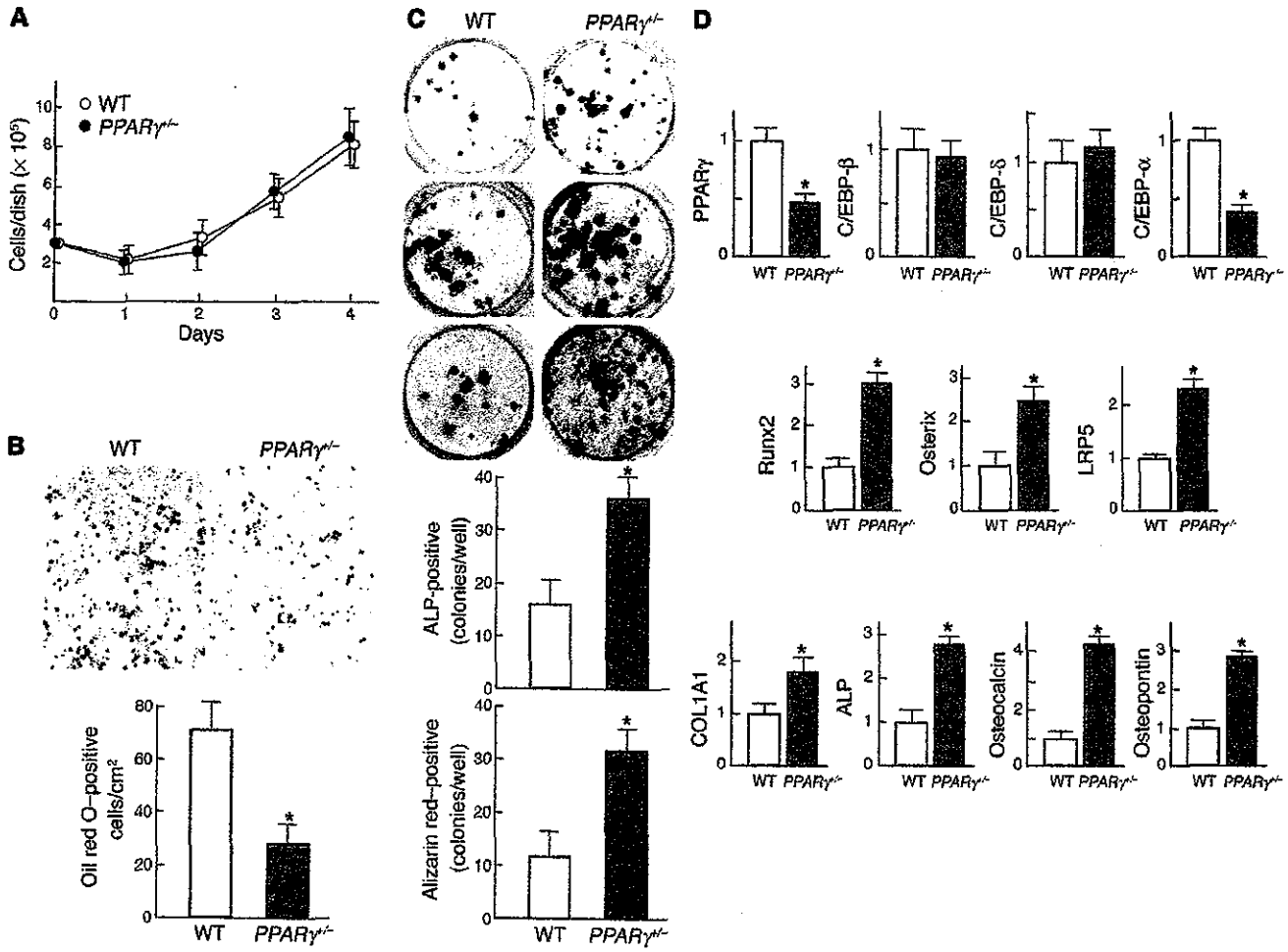

Figure 5

Adipogenesis and osteogenesis in the cultures of bone marrow cells from *PPARγ*$^{-/-}$ and WT littermates. (**A**) Growth curves of bone marrow cells isolated from *PPARγ*$^{-/-}$ and WT mice. The adherent bone marrow cells were inoculated at a density of 3×10^5 cells/dish in 10-cm culture dishes. The cells per dish were counted at 1, 2, 3, and 4 days of culture. Data are expressed as means (symbols) ± SEMs (error bars) for eight dishes per group. (**B**) Adipogenesis determined by oil red O staining in the culture of bone marrow cells in α-MEM/10% FBS with troglitazone. The graph indicates the number of positive cells per square centimeter. (**C**) Osteogenesis determined by ALP (upper row), Alizarin red (middle row), and von Kossa (lower row) stainings in the culture of bone marrow cells in α-MEM/10% FBS with ascorbic acid and β-glycerophosphate. The graphs below indicate the number of ALP-positive (upper) and Alizarin red–positive (lower) colonies per well. Data are expressed as means (bars) ± SEMs (error bars) for eight wells per group (**B** and **C**). *Significant difference from the WT culture, $P < 0.01$. (**D**) Expression of key molecules for adipogenesis (PPARγ, C/EBP-β, C/EBP-δ, and C/EBP-α) and osteogenesis (Runx2, osterix, and LRP5), and marker proteins for osteogenesis (COL1A1, ALP, osteocalcin, and osteopontin) determined by quantitative RT-PCR in the bone marrow cells at 14 days of culture under the conditions above. The ordinate axis indicates the relative amount of mRNA as compared with that of WT.

regulated, at least in part, downstream of PPARγ. Regarding osteogenic factors, expressions of the putative central determinants of major pathways for osteoblast differentiation, Runx2 (34), osterix (35), and LDL receptor–related protein 5 (LRP5) (36), were increased in the *PPARγ*$^{-/-}$ culture as compared with WT, indicating that the PPARγ signaling directly or indirectly impacts these major pathways for osteoblast differentiation. Expressions of matrix proteins representing osteogenesis, COL1A1, ALP, osteocalcin, and osteopontin, were also higher in the *PPARγ*$^{-/-}$ culture than in the WT culture, which was consistent with the in vivo histomorphometric data showing high bone mass with increased osteoblastogenesis.

When we examined the proliferation, differentiation, and matrix synthesis of cultured calvarial osteoblasts, which we confirmed to be more mature than bone marrow cells, none of them showed a difference between *PPARγ*$^{-/-}$ and WT mice (data not shown). This indicates that PPARγ haploinsufficiency affects only marrow progenitors, but not cells that are more committed to osteoblastic lineage. Furthermore, studies using the coculture system of marrow cells/calvarial osteoblasts and the M-BMMϕ culture system (28, 37) also failed to show difference of differentiation, bone-resorbing activity, or survival of the osteoclastic cells, suggesting that PPARγ is not important for osteoclast functions.

Discussion

Osteoblastogenesis was upregulated not only in the *PPARγ*$^{-/-}$ bone in vivo, but also in the cultures of *PPARγ*$^{-/-}$ ES cells and *PPARγ*$^{-/-}$

primary bone marrow cells. Considering that the former culture was performed in the absence of any osteogenic stimulation, under which condition no WT stem cells can differentiate into osteoblasts, the intrinsic PPARγ signaling seems to function as a potent suppressor of commitment and differentiation to the osteoblastic lineage. Its molecular mechanism remains unclear, however. A previous report showed that a stable transfection of PPARγ and its activation with a thiazolidinedione-suppressed Runx2, type I collagen, and osteocalcin syntheses in the culture of a stromal cell line (38). Although the present study also showed that steady-state mRNA levels of the key molecules for osteoblast differentiation, Runx2, osterix, and LRP5, were upregulated in primary cultured marrow cells with PPARγ haploinsufficiency (Figure 5D), whether this is transcriptional regulation or secondary to the increase in cells of osteoblast lineage in the culture is unknown. The predicted region of the PPARγ-responsive element PPRE (TGACCTnTGACCT) has not been identified in the promoter of these genes and was not found by our genomic search, at least in the region between 4.0 kb upstream and 0.5 kb downstream of the transcriptional start point of *runx2* (GenBank accession number NT 039655), *osterix* (NT 039621), and *lrp5* (NT 039684) genes. It should, however, also be noted that several reports have indicated that PPARγ regulates gene expression independently of PPRE, that is, by interfering with the function of AP-1, signal transducer and activator of transcription 1 (STAT1), and NF-κB (39), or by inhibiting the function of GHP-1, a transcription factor implicated in pituitary-specific gene expression (40). The AP-1 family members may possibly play a role in the mechanism, especially for mesenchymal cells. Activation of PPARγ is reported to suppress *c-fos* expression (41). Another AP-1 family member, DeltaFosB, is known to be a positive regulator of osteoblast differentiation, and the transgenic mouse leads to postnatal high bone mass with increased osteoblastogenesis and decreased adipogenesis in bone marrow (12). Another possible molecular mechanism is the interaction of PPARγ with the TGF-β/Smad3 signaling, which inhibits osteoblast differentiation (42, 43). Since Smad3 is reported to interact physically with Runx2 (42) and PPARγ (44), the interference by PPARγ with the Smad3 inhibition of Runx2 might be involved in the switching mechanism between adipocyte and osteoblast differentiation. The interaction of PPARγ with Wnt signaling might be another issue to pursue. The canonical Wnt pathway, likely mediated by Wnt10b, is known to maintain preadipocytes in an undifferentiated state through stabilization of cytosolic β-catenin (45, 46). Since activation of PPARγ with troglitazone is not sufficient to repress expression of Wnt10b, Wnt signaling might lie upstream of PPARγ. Recently, in addition to LRP5, which is a coreceptor of Wnt, the canonical Wnt-signaling molecules β-catenin and glycogen synthase kinase-3β have been reported to stimulate osteoblast differentiation (47, 48), indicating a switching between adipogenesis and osteogenesis by the Wnt signaling. Further studies on functional interaction of PPARγ with the transcriptional and signaling molecules above will elucidate the switching mechanism between the two differentiation pathways from common progenitors.

PPARγ may also inhibit osteogenesis indirectly through its stimulation of adipogenesis from marrow progenitors that can give rise to either osteoblasts or adipocytes. In fact, many experimental models have provided substantial evidence for this reciprocal relationship between cell lineages (6, 10–15), and there is little doubt that adipogenesis increases as BV decreases, suggesting that marrow adipogenesis has important implications in osteogenic disorders (7–9). Evidence of the transdifferentiation of stromal cells actually suggests a large degree of plasticity between osteoblasts and adipocytes (4, 49), although it is not clear at what point the phenotype of these multipotential cells becomes committed to either osteoblast or adipocyte differentiation. Since differentiated osteoblasts indicated by osteocalcin expression are reported to undergo adipogenic differentiation (4), it is possible that the reciprocal relationship between osteogenesis and adipogenesis may, at least in part, be due to the transdifferentiation between rather differentiated cells of the two lineages. To determine the role of PPARγ in more differentiated osteoblastic cells than bone marrow cells, we used calvarial cells whose spontaneous differentiation is known to follow not only the osteogenic pathway but also the adipogenic pathway (49). Despite the existence of PPARγ expression in these cells as well, its haploinsufficiency did not affect the cell functions, suggesting that PPARγ signaling may be involved in the earlier, but not the later, stage of relationship between the two cell lineages.

Hormones regulating bone and fat metabolisms include insulin and leptin, both of which are known to be related to the PPARγ signaling. Insulin is known to play important anabolic roles in bone (30), and deficiency of insulin signaling is associated with osteopenia both in mice and humans (27, 50–52). A series of reports demonstrated that leptin, a well-known anorexigenic hormone secreted by adipocytes (53), also shows antiosteogenic action centrally through the hypothalamic and sympathetic nervous systems (11, 13, 31). In the present study, neither insulin nor leptin seemed to mediate the high bone mass in *PPARγ*$^{+/-}$ mice, since the serum levels of these hormones were, quite unexpectedly, the opposite of those causing osteogenic functions. PPARγ activation is known to cause insulin sensitivity, thus *PPARγ*$^{+/-}$ mice were assumed to develop insulin resistance; however, the serum insulin level was normal or somewhat decreased as previously reported (22, 29). This appears, at least in part, due to hypersecretion of leptin, which was also unexpected, given that the marrow adipocytes, a positive regulator of leptin expression, were decreased in *PPARγ*$^{+/-}$ mice. Our previous studies clearly demonstrated that cultured primary adipocytes from *PPARγ*$^{+/-}$ mice expressed and secreted increased levels of leptin as compared with those from WT (22, 29). In this respect, since leptin is known to have a functional PPRE whose activity is suppressed by PPARγ activation in adipocytes (54, 55), it is likely that the increased level of leptin is due to a partial release from the suppressive effect of PPARγ on leptin gene transcription by loss of one *PPARγ* allele.

Age-related bone loss has been suggested to be attributable to increased adipogenesis at the expense of osteoblastogenesis (7–9). Indeed, studies of SAMP6 mice, a murine model of age-related osteopenia, have established a tight association between osteopenia and enhanced adipogenesis (10, 15). The fact that the effects of PPARγ haploinsufficiency on both the increase in bone volume and the decrease in adipocytes were stronger at 52 weeks than at 8 weeks suggests the involvement of the PPARγ signaling in the pathophysiology of human age-related osteoporosis. In fact, our preliminary examination of the bone marrow specimen from patients with femoral neck fracture actually showed increases of both the PPARγ mRNA level and fat mass in older patients (data not shown) as compared with those in younger patients, although the causality between PPARγ level and adipogenesis remains unknown since adipocytes can be both the source and the target

of PPARγ. An association study between bone density and a genetic polymorphism of *PPARγ* in postmenopausal women implies the involvement of PPARγ in bone loss, although the functional relevance remains unclear (56). We should, however, keep in mind that there are two distinct factors that determine involutional osteoporosis: a rapid bone loss after menopause as a result of estrogen withdrawal and a gradual age-related bone loss thereafter (57). From the present study showing that PPARγ insufficiency did not affect bone loss by OVX, PPARγ may not be involved in the former stage, but may play a role in the latter. To confirm the involvement of PPARγ in human osteoporosis, the next task ahead of us will be to perform a genetic association study with stratified analysis by age and menopausal state, and more importantly, to use a cohort population.

We conclude herein that PPARγ haploinsufficiency leads to the increase of bone mass by stimulating osteoblastogenesis from bone marrow progenitors without affecting differentiated osteoblasts or osteoclast lineage cells. Based on the present and previous evidence presented, we believe that PPARγ may be a novel target for therapeutic intervention of osteopenic disorders, although the mechanism remains to be clarified. Appropriate functional antagonism of PPARγ may provide a potentially novel approach to increasing bone formation and therefore, as a stand-alone therapy or in combination with an antiresorptive medication, may provide more efficacious prevention or treatment of osteoporosis.

Acknowledgments

We thank the hard tissue research team at Kureha Chemical Co. for technical assistance. We are grateful to Bruce M. Spiegelman for the pBabe-mPPARγ2-puro vector. This work was supported by Grants-in-Aid for Scientific Research from the Japanese Ministry of Education, Culture, Sports, Science, and Technology (1370303) and the ONO Medical Research Foundation.

Received for publication August 28, 2003, and accepted in revised form January 6, 2004.

Address correspondence to: Hiroshi Kawaguchi, Department of Orthopaedic Surgery, Faculty of Medicine, University of Tokyo, Hongo 7-3-1, Bunkyo-ku, Tokyo 113-8655, Japan. Phone: 81-33815-5411 ext. 30473 or 33376; Fax: 81-33818-4082; E-mail: kawaguchi-ort@h.u-tokyo.ac.jp.

1. Beresford, J.N. 1989. Osteogenic stem cells and the stromal system of bone and marrow. *Clin. Orthop.* **240**:270–280.
2. Pittenger, M.F., et al. 1999. Multilineage potential of adult human mesenchymal stem cells. *Science.* **284**:143–147.
3. Bennett, J.H., Joyner, C.J., Triffitt, J.T., and Owen, M.E. 1991. Adipocytic cells cultured from marrow have osteogenic potential. *J. Cell Sci.* **99**:131–139.
4. Nuttall, M.E., Patton, A.J., Olivera, D.L., Nadeau, D.P., and Gowen, M. 1998. Human trabecular bone cells are able to express both osteoblastic and adipocytic phenotype: implications for osteopenic disorders. *J. Bone Miner. Res.* **13**:371–382.
5. Park, S.R., Oreffo, R.O., and Triffitt, J.T. 1999. Interconversion potential of cloned human marrow adipocytes in vitro. *Bone.* **24**:549–554.
6. Beresford, J.N., Bennett, J.H., Devlin, C., Leboy, P.S., and Owen, M.E. 1992. Evidence for an inverse relationship between the differentiation of adipocytic and osteogenic cells in rat marrow stromal cell cultures. *J. Cell Sci.* **102**:341–351.
7. Meunier, P., Aaron, J., Edouard, C., and Vignon, G. 1971. Osteoporosis and the replacement of cell populations of the marrow by adipose tissue. A quantitative study of 84 iliac bone biopsies. *Clin. Orthop.* **80**:147–154.
8. Burkhardt, R., et al. 1987. Changes in trabecular bone, hematopoiesis and bone marrow vessels in aplastic anemia, primary osteoporosis, and old age: a comparative histomorphometric study. *Bone.* **8**:157–164.
9. Rozman, C., et al. 1989. Age-related variations of fat tissue fraction in normal human bone marrow depend both on size and number of adipocytes: a stereological study. *Exp. Hematol.* **17**:34–37.
10. Jilka, R.L., Weinstein, R.S., Takahashi, K., Parfitt, A.M., and Manolagas, S.C. 1996. Linkage of decreased bone mass with impaired osteoblastogenesis in a murine model of accelerated senescence. *J. Clin. Invest.* **97**:1732–1740.
11. Ducy, P., et al. 2000. Leptin inhibits bone formation through a hypothalamic relay: a central control of bone mass. *Cell.* **100**:197–207.
12. Sabatakos, G., et al. 2000. Overexpression of DeltaFosB transcription factor(s) increases bone formation and inhibits adipogenesis. *Nat. Med.* **6**:985–990.
13. Takeda, S., et al. 2002. Leptin regulates bone formation via the sympathetic nervous system. *Cell.* **111**:305–317.
14. Takeuchi, Y., et al. 2002. Interleukin-11 as a stimulatory factor for bone formation prevents bone loss with advancing age in mice. *J. Biol. Chem.* **277**:49011–49018.
15. Kodama, Y., et al. 1998. Reduced expression of interleukin-11 in bone marrow stromal cells of senescence-accelerated mice (SAMP6): relationship to osteopenia with enhanced adipogenesis. *J. Bone Miner. Res.* **13**:1370–1377.
16. Rosen, E.D., Walkey, C.J., Puigserver, P., and Spiegelman, B.M. 2000. Transcriptional regulation of adipogenesis. *Genes Dev.* **14**:1293–1307.
17. Rosen, E.D., and Spiegelman, B.M. 2001. PPARγ: a nuclear regulator of metabolism, differentiation, and cell growth. *J. Biol. Chem.* **12**:37731–37734.
18. Kersten, S., Desvergne, B., and Wahli, W. 2000. Roles of PPARs in health and disease. *Nature.* **405**:421–424.
19. Mangelsdorf, D.J., and Evans, R.M. 1995. The RXR heterodimers and orphan receptors. *Cell.* **83**:841–850.
20. Tontonoz, P., Hu, E., and Spiegelman, B.M. 1994. Stimulation of adipogenesis in fibroblasts by PPAR γ 2, a lipid-activated transcription factor. *Cell.* **79**:1147–1156.
21. Barak, Y., et al. 1999. PPAR γ is required for placental, cardiac, and adipose tissue development. *Mol. Cell.* **4**:585–595.
22. Kubota, N., et al. 1999. PPAR γ mediates high-fat diet-induced adipocyte hypertrophy and insulin resistance. *Mol. Cell.* **4**:597–609.
23. Rosen, E.D., et al. 1999. PPAR γ is required for the differentiation of adipose tissue in vivo and in vitro. *Mol. Cell.* **4**:611–617.
24. Kadowaki, T. 2000. Insights into insulin resistance and type 2 diabetes from knockout mouse models. *J. Clin. Invest.* **106**:459–465.
25. Bradley, A. 1987. Production and analysis of chimaeric mice. In *Teratocarcinomas and embryonic stem cells.* E.J. Robertson, editor. IRL Press. Oxford, United Kingdom. 113–151.
26. Keller, G.M. 1995. In vitro differentiation of embryonic stem cells. *Curr. Opin. Cell Biol.* **7**:862–869.
27. Akune, T., et al. 2002. Insulin receptor substrate-2 maintains predominance of anabolic function over catabolic function of osteoblasts. *J. Cell Biol.* **159**:147–156.
28. Kobayashi, K., et al. 2000. Tumor necrosis factor α stimulates osteoclast differentiation by a mechanism independent of the ODF/RANKL-RANK interaction. *J. Exp. Med.* **191**:275–286.
29. Yamauchi, T., et al. 2001. The mechanisms by which both heterozygous peroxisome proliferator-activated receptor γ (PPARγ) deficiency and PPARgamma agonist improve insulin resistance. *J. Biol. Chem.* **276**:41245–41254.
30. Thomas, D.M., Hards, D.K., Rogers, S.D., Ng, K.W., and Best, J.D. 1997. Insulin and bone, clinical and scientific view. *Endocrinology and Metabolism.* **4**:5–17.
31. Takeda, S., and Karsenty, G. 2001. Central control of bone formation. *J. Bone Miner. Metab.* **19**:195–198.
32. Tanaka, T., Yoshida, N., Kishimoto, T., and Akira, S. 1997. Defective adipocyte differentiation in mice lacking the C/EBPβ and/or C/EBPδ gene. *EMBO J.* **16**:7432–7443.
33. Wu, Z., et al. 1999. Cross-regulation of C/EBP α and PPAR γ controls the transcriptional pathway of adipogenesis and insulin sensitivity. *Mol. Cell.* **3**:151–158.
34. Karsenty, G. 2001. Minireview: transcriptional control of osteoblast differentiation. *Endocrinology.* **142**:2731–2733.
35. Nakashima, K., et al. 2002. The novel zinc finger-containing transcription factor osterix is required for osteoblast differentiation and bone formation. *Cell.* **108**:17–29.
36. Patel, M.S., and Karsenty, G. 2002. Regulation of bone formation and vision by LRP5. *N. Engl. J. Med.* **346**:1572–1574.
37. Suda, T., et al. 1999. Modulation of osteoclast differentiation and function by the new members of the tumor necrosis factor receptor and ligand families. *Endocr. Rev.* **20**:345–357.
38. Lecka-Czernik, B., et al. 1999. Inhibition of Osf2/Cbfa1 expression and terminal osteoblast differentiation by PPARγ2. *J. Cell. Biochem.* **74**:357–371.
39. Ricote, M., Li, A.C., Willson, T.M., Kelly, C.J., and Glass, C.K. 1998. The peroxisome proliferator-activated receptor-γ is a negative regulator of macrophage activation. *Nature.* **391**:79–82.
40. Tolon, R.M., Castillo, A.I., and Aranda, A. 1998. Activation of the prolactin gene by peroxisome proliferator-activated receptor-α appears to be DNA binding-independent. *J. Biol. Chem.* **273**:26652–26661.
41. Benson, S., Wu, J., Padmanabhan, S., Kurtz, T.W., and Pershadsingh, H.A. 2000. Peroxisome proliferator-activated receptor (PPAR)-γ expression in human vascular smooth muscle cells: inhibition of growth, migration, and c-fos expression by the peroxisome proliferator-activated receptor (PPAR)-γ activator troglitazone. *Am. J. Hypertens.* **13**:74–82.
42. Alliston, T., Choy, L., Ducy, P., Karsenty, G., and

Derynck, R. 2001. TGF-β-induced repression of CBFA1 by Smad3 decreases cbfa1 and osteocalcin expression and inhibits osteoblast differentiation. *EMBO J.* **20**:2254–2272.
43. Borton, A.J., Frederick, J.P., Datto, M.B., Wang, X.F., and Weinstein, R.S. 2001. The loss of Smad3 results in a lower rate of bone formation and osteopenia through dysregulation of osteoblast differentiation and apoptosis. *J. Bone Miner. Res.* **16**:1754–1764.
44. Fu, M., et al. 2001. Peroxisome proliferator-activated receptor γ inhibits transforming growth factor beta-induced connective tissue growth factor expression in human aortic smooth muscle cells by interfering with Smad3. *J. Biol. Chem.* **276**:45888–45894.
45. Ross, S.E., et al. 2000. Inhibition of adipogenesis by Wnt signaling. *Science.* **289**:950–953.
46. Bennett, C.N., et al. 2002. Regulation of Wnt signaling during adipogenesis. *J. Biol. Chem.* **277**:30998–31004.
47. Bain, G., Muller, T., Wang, X., and Papkoff, J. 2003. Activated β-catenin induces osteoblast differentiation of C3H10T1/2 cells and participates in BMP2 mediated signal transduction. *Biochem. Biophys. Res. Commun.* **301**:84–91.
48. Smith, E., Coetzee, G.A., and Frenkel, B. 2002. Glucocorticoids inhibit cell cycle progression in differentiating osteoblasts via glycogen synthase kinase-3β. *J. Biol. Chem.* **277**:18191–18197.
49. Garcia, T., et al. 2002. Behavior of osteoblast, adipocyte, and myoblast markers in genome-wide expression analysis of mouse calvaria primary osteoblasts in vitro. *Bone.* **31**:205–211.
50. Krakauer, J.C., McKenna, M.J., Rao, D.S., and Whitehouse, F.W. 1997. Bone mineral density in diabetes. *Diabetes Care.* **20**:1339–1340.
51. Piepkorn, B., et al. 1997. Bone mineral density and bone metabolism in diabetes mellitus. *Horm. Metab. Res.* **29**:584–591.
52. Ogata, N., et al. 2000. Insulin receptor substrate-1 in osteoblast is indispensable for maintaining bone turnover. *J. Clin. Invest.* **105**:935–943.
53. Elmquist, J.K., Elias, C.F., and Saper, C.B. 1999. From lesions to leptin: hypothalamic control of food intake and body weight. *Neuron.* **22**:221–232.
54. Kallen, C.B., and Lazar, M.A. 1996. Antidiabetic thiazolidinediones inhibit leptin (ob) gene expression in 3T3-L1 adipocytes. *Proc. Natl. Acad. Sci. U. S. A.* **93**:5793–5796.
55. Hollenberg, A.N., et al. 1997. Functional antagonism between CCAAT/enhancer binding protein-α and peroxisome proliferator-activated receptor-γ on the leptin promoter. *J. Biol. Chem.* **272**:5283–5290.
56. Ogawa, S., et al. 1999. Association of bone mineral density with a polymorphism of the peroxisome proliferator-activated receptor γ gene: PPARγ expression in osteoblasts. *Biochem. Biophys. Res. Commun.* **260**:122–126.
57. Nguyen, T.V., Blangero, J., and Eisman, J.A. 2000. Genetic epidemiological approaches to the search for osteoporosis genes. *J. Bone Miner. Res.* **15**:392–401.

Available online at www.sciencedirect.com
SCIENCE DIRECT®
Biomaterials 25 (2004) 1115–1122
Biomaterials
www.elsevier.com/locate/biomaterials

Polyethylene/phospholipid polymer alloy as an alternative to poly(vinylchloride)-based materials

Kazuhiko Ishihara[a,*], Daisuke Nishiuchi[a], Junji Watanabe[a], Yasuhiko Iwasaki[b]

[a] *Department of Materials Engineering, The University of Tokyo, Hongo, Bunkyo-ku, Tokyo 113-8656, Japan*
[b] *Institute of Biomaterials and Bioengineering, Tokyo Medical and Dental University, Kanda-surugadai, Chiyoda-ku, Tokyo 162-0022, Japan*

Received 5 June 2003; accepted 10 July 2003

Abstract

To develop new biomaterials for making medical devices, polymer alloys composed of a phospholipid polymer, poly(2-methacryloyloxyethyl phosphorylcholine) (PMPC), and polyethylene (PE) were prepared. The PE/PMPC alloy membrane could be obtained by a combination of solution mixing and solvent evaporation methods using xylene and *n*-butanol mixture as a solvent. Moreover, thermal treatment was applied to improve the mechanical properties of the PE/PMPC alloy membrane. In the PE/PMPC alloy membrane, the PMPC domains were located not only inside the membrane but also at the surface. Surface analysis of the PE/PMPC alloy membrane with X-ray photoelectron spectroscopy, wettability evaluation, and dynamic contact angle measurements revealed that the phospholipid polar groups in the PMPC covered the surface even after thermal treatment. Blood compatibility tests with attention to platelet adhesion and change in morphology of adhered platelets showed that the PE/PMPC alloy membrane had excellent platelet adhesion resistance. We finally concluded that the PE/PMPC alloy could be used as biomaterials instead of poly(vinyl chloride)-based materials.

Keywords: 2-methacryloyloxyethyl phosphorylcholine polymer; Polyethylene; Polymer alloy; Domain structure; Wettability; Platelet adhesion resistance

1. Introduction

To avoid infection from medical devices, many single-use medical devices, such as catheters, connecting tubings, and bags are now used. How to dispose of these single-use medical devices after treatment is currently a big environmental problem. Most of these disposable medical devices are made from soft-type polymer materials composed of poly(vinyl chloride) (PVC) and a plasticizer. This material contains 70 wt% plasticizer, which may be a hormone-like chemical. Moreover, chlorine in PVC has the possibility of forming dioxin during burning. Thus, some substitutions, so-called green materials, are needed. Polyethylene (PE) is a conventional polymer and is very inert chemically; no harmful chemicals are produced even when it is burned. Because the mechanical properties and processability of PE are good, it has been used as a liner in artificial hip joints [1]. However, when it contacts blood, thrombus is formed on the PE very easily. If the biocompatibility of PE could be improved without loss of its mechanical properties and processability, application of modified-PE would be used much more for biomaterials.

Recently, we prepared several polymer alloys composed of conventional polymers and biocompatible phospholipid polymers, 2-methacryloyloxyethyl phosphorylcholine (MPC) polymers [2–7]. That is, an MPC polymer alloy with segmented polyurethane (SPU) could be processed as a small diameter vascular prosthesis, and it functioned in vivo [2,3]. Another significant polymer alloy is composed of the MPC polymer and polysulfone (PSf), and hollow fibers for blood purification could be prepared from the polymer alloy [4,5]. We tried to prepare a new polymer alloy composed of PE and MPC polymer (PE/MPC polymer alloy). PE is apolar and crystalline, so it is very difficult to blend such a polar MPC polymer in the PE. In this study, we investigated the preparation and

*Corresponding author.
E-mail address: ishihara@bmw.t.u-tokyo.ac.jp (K. Ishihara).

0142-9612/$ - see front matter © 2003 Elsevier Ltd. All rights reserved.
doi:10.1016/S0142-9612(03)00624-0

characterization of a PE/MPC polymer alloy membrane and its platelet adhesion resistance.

2. Experimental

2.1. Materials

PE was obtained from Aldrich ($M_w = 1.0 \times 10^5$) and used without further purification. Homopolymer of MPC (PMPC, Fig. 1) was prepared by a conventional radical polymerization of MPC in ethanol and purified by reprecipitation with a diethylether/chloroform mixture [8]. The weight-averaged molecular weight of the PMPC obtained was 5.4×10^4, which was determined by gel-permeation chromatography with poly(ethylene glycol) standards in water. Other solvents and reagents were extra-pure reagent-grade and were used without further purification.

2.2. Preparation of PE/MPC polymer alloy membrane

The PE/PMPC alloy membrane was prepared by a combination of solution mixing and solvent evaporation methods. The procedure is shown in Fig. 2. PE was dissolved in xylene at 110°C for 1 h. The PE solution was cooled at room temperature. The PMPC was dissolved in *n*-butanol, and the solution was mixed with the PE solution. After stirring, the mixed solution was heated and maintained for 5 h at 110°C. The polymer solution was poured onto a glass plate, and the solvents were evaporated under reduced pressure at 25°C/160 mmHg overnight. The residual solvents were then removed completely by vacuum drying. A light opaque polymer membrane was obtained. Heat treatment was applied at a given temperature for 5 min under pressure at 2 MPa.

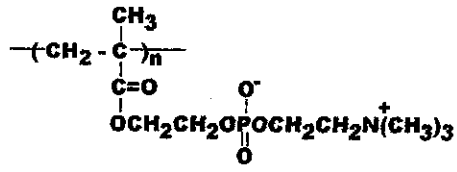

Fig. 1. Chemical structure of poly(2-methacryloyloxyethyl phosphorylcholine) (PMPC).

2.3. Analysis of PE/PMPC alloy membrane

Elution of PMPC from the PE/PMPC alloy membrane was evaluated when the membrane was immersed in water at 30°C for 1 week. The amount of PMPC was determined by phosphorus analysis. The sensitivity of this analysis for phosphate ion is 10^{-10} mol/l levels [4].

Thermal properties were investigated by differential scanning calorimetory (DSC 6100, Seiko Instruments Co., Chiba, Japan). The measurement was scanned at 5°C/min over the temperature range of 20–200°C. Surface analysis was carried out by X-ray photoelectron spectroscopy (XPS, ESCA-200, Scienta, Uppsala, Sweden). The dynamic contact angle (DCA) hysteresis loop of the polymer membrane was recorded with a computer-controlled dynamic contact angle meter (DCA-100, Orientech, Tokyo, Japan) based on the Wilhelmy plate method. The DCA loop was expressed by plotting the interfacial tension against the immersion depth of the sample polymer membrane. The DCA loops were obtained three times repeatedly for one membrane of each sample, and the averaged values of the advancing contact angle, θ_A, and receding contact

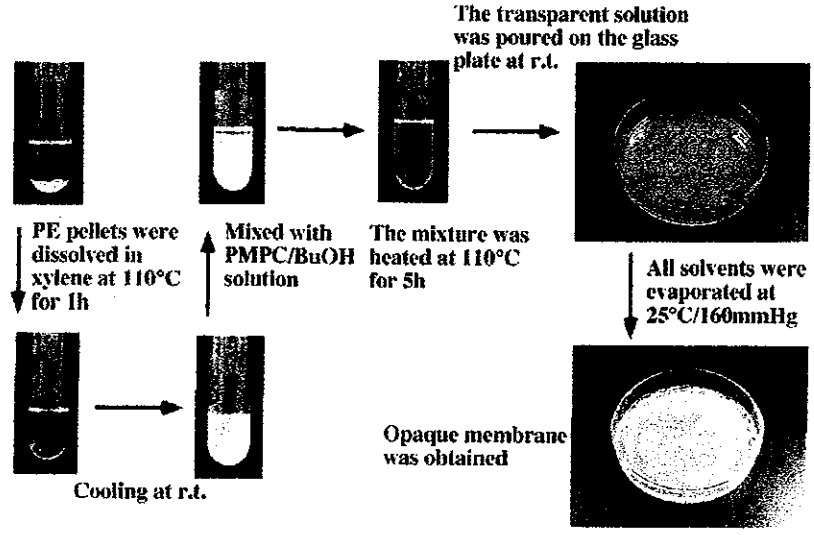

Fig. 2. Procedure for preparing PE/PMPC alloy membrane.